

This item is the archived peer-reviewed author-version of:

Physical plasma-derived oxidants sensitize pancreatic cancer cells to ferroptotic cell death

Reference:

Kumar Naresh, Perez Novo Claudina, Shaw Priyanka, Logie Emilie, Privat-Maldonado Angela, Dewilde Sylvia, Smits Evelien, Vanden Berghe Wim, Bogaerts Annemie.- Physical plasma-derived oxidants sensitize pancreatic cancer cells to ferroptotic cell death
Free radical biology and medicine - ISSN 0891-5849 - 166(2021), p. 187-200
Full text (Publisher's DOI): <https://doi.org/10.1016/J.FREERADBIOMED.2021.02.026>
To cite this reference: <https://hdl.handle.net/10067/1768780151162165141>

Physical plasma-derived oxidants sensitize pancreatic cancer cells to ferroptotic cell death

Naresh Kumar^{1,4&}, Claudina Perez-Novo^{2&}, Priyanka Shaw^{1,3&}, Emilie Logie², Angela Privat-Maldonado^{1,3}, Sylvia Dewilde², Evelien Smits³, Wim Vanden Berghe^{2*} and Annemie Bogaerts,^{1*}*

¹ Research group PLASMANT, Department of Chemistry, University of Antwerp, Antwerp-2610, Belgium

²Department of Biomedical Sciences, Laboratory of Protein Science, Proteomics & Epigenetic Signalling, University of Antwerp, Antwerp-2610, Belgium.

³Solid Tumor Immunology Group, Center for Oncological Research, University of Antwerp - 2610, Belgium.

⁴National Institute of Pharmaceutical Education and Research, Guwahati, -781125, Guwahati, Assam, India.

& These authors equally contributed to this work

*Correspondence to: nash.bms@gmail.com, annemie.bogaerts@uantwerpen.be & wim.vandenbergh@uantwerpen.be

Abstract

Despite modern therapeutic advances, the survival prospects of pancreatic cancer patients remain poor, due to chemoresistance and dysregulated oncogenic kinase signalling networks. We applied a novel kinome activity-mapping approach using biological peptide targets as phospho-sensors to identify vulnerable kinase dependencies for therapy sensitisation by physical plasma. Ser/Thr-kinome specific activity changes were mapped upon induction of ferroptotic cell death in pancreatic tumor cells exposed to reactive oxygen and nitrogen species of plasma-treated water (PTW). This revealed a broad kinome activity response involving the CAMK, the AGC and CMGC family of kinases. This systems-level kinome network response supports stress adaptive switches between chemoresistant anti-oxidant responses of Kelch-like ECH-associated protein 1 (KEAP1)/ Heme Oxygenase 1 (HMOX1) and ferroptotic cell death sensitisation upon suppression of Nuclear factor (erythroid derived 2)-like 2 (NRF2) and Glutathione peroxidase 4 (GPX4). This is further supported by *ex vivo* experiments in the chicken chorioallantoic membrane assay, showing decreased GPX4 and Glutathione (GSH) expression as well as increased lipid peroxidation, along with suppressed BxPC-3 tumor growth in response to PTW. Taken all together, we demonstrate that plasma treated water-derived oxidants sensitize pancreatic cancer cells to ferroptotic cell death by targeting a NRF2-HMOX1-GPX4 specific kinase signaling network.

Keywords: Pancreatic cancer, ferroptosis, oxidative stress, reactive oxygen and nitrogen species, Serine/Threonine protein kinases

1. Introduction

Pancreatic ductal adenocarcinoma (PDAC), generally known as pancreatic cancer, represents the fourth leading cause of cancer-related deaths in the western world. While the incidence of this disease is displaying a rising tendency every year, the mortality rate has not decreased significantly because of late diagnosis, early metastasis, and poor clinical therapy response [1]. It is well known that a major contributor to this poor clinical outcome is the prominent chemoresistance, which is triggered by the resistance of pancreatic cells to undergo apoptosis. Besides, the unique tumor microenvironment where cancer cells cross-talk with pancreatic stellate cells promotes an intrastromal and intratumoral hypoxia cycle impairing drug delivery to cancer cells, as well as (epi)genetic instability of pancreatic cells. Frequently this involves dysregulation of kinase signalling networks. The coordinated regulation of protein kinases is a dynamic mechanism that translates diverse stress cues into cytoprotective drug resistant or cytotoxic drug responses [2]. Upon oxidative chemotherapeutic stress signaling, NRF2 becomes typically unleashed from KEAP1 binding and translocates to the nucleus. There, NRF2 binds to antioxidant responsive element (ARE) and activates genes in order to balance oxidative mediators and maintain cellular redox homeostasis [3]. KEAP1 can turn the NRF2-mediated response on and off, dependent on the intracellular redox status. Alternatively, imbalanced redox consumption and NRF2 overexpression by oncogenic alleles (i.e. K-Ras, B-Raf and Myc) in pancreatic cancer cells increases cell proliferation and causes epithelial-mesenchymal transition, which result in tumor progression, metastasis and chemoresistance [4]. This has fueled the search for therapeutic strategies targeting alternative (non-apoptotic) types of programmed cell death, such as necrosis/necroptosis or ferroptosis [5]. Cancer cells exhibit an increased iron demand compared with normal, non-cancer cells to enable growth. This iron dependency can make cancer cells more vulnerable to iron-catalyzed necrosis, referred to as ferroptosis. The identification of FDA-approved drugs as ferroptosis inducers creates high expectations towards ferroptosis as a new strategy to kill therapy-resistant cancers [6]. The cystine/glutamate antiporter inhibitor erastin was originally described to induce various ferroptosis hallmarks by increasing iron, lipid reactive oxygen species (ROS), and reducing the glutathione synthesis [6-9]. Interestingly, besides chemical ferroptosis induction, plasma treatment was recently also discovered to promote ferroptosis in cancer cells via the reduction of ferritin stored Fe^{3+} to Fe^{2+} , lipid peroxidation in the cytoplasm, which thus directly or indirectly indicates that plasma shows similar efficacy to erastin-induced ferroptosis [10, 11]. Physical plasma is a partially ionized gas that contains a mixture of highly reactive oxygen and

nitrogen species (RONS), such as $\cdot\text{OH}$, $\text{O}_2^{\cdot-}$, $\text{NO}\cdot$, NO_2^- , NO_3^- and H_2O_2 [12]. Accumulation of reactive species surrounding a biological target results in excessive peroxidation of polyunsaturated fatty acids (PUFAs) [13]. These play a key role in regulating non-apoptotic cell death mechanisms, such as ferroptosis characterized by iron-dependent accumulation of lipid peroxides, mainly caused by an impaired redox balance [14]. Moreover, RONS induction by plasma-treated liquids (PTLs), e.g., culture media, saline solutions and phosphate buffers, showed promising therapeutic efficacy against drug resistant cancers, such as glioblastomas, lung cancer, leukaemia, melanoma, and pancreatic adenocarcinomas, and have received a growing scientific interest [13, 15, 16].

Previously, we showed that the presence of amino acids, fetal bovine serum, pyruvate and inorganic salts in these preparations have significant impact on the production of RONS, the stability and hence anti-tumor efficacy of these preparations [17]. In the present study, we further focus on plasma-treated (deionised) water (PTW), which allows a more reproducible generation of RONS. Indeed, one of the central advantages of plasma-treated deionized water is to reduce the pH value, which supports the generation of highly potent radicals, such as superoxide anion ($\text{O}_2^{\cdot-}$), hydroxyl radical, ($\cdot\text{OH}$), protonated peroxyxynitrite (ONOO^-), i.e., either carboxylate acid (ONOOH) or peroxyxynitric acid (O_2NOOH), hydrogen peroxide (H_2O_2), nitrite (NO_2^-) and nitrate (NO_3^-) ions [18-20], etc. Among these radicals $\cdot\text{OH}$ and ONOO^- directly interact with the cell membrane and cause increased level of Fe^{2+} and lipid peroxidation, which eventually induces ferroptosis through depletion of GSH/GPX4 [10, 11, 13,]. More particularly, ferroptosis sensitisation of chemoresistant adenocarcinoma pancreatic cell lines by plasma-treated water (PTW) was studied in different *in vitro*, *ex vivo* (*in ovo*) cell models, and analysed by *in silico* molecular dynamic simulations, as well as phospho- peptidome based kinome assays, in relation to the oxidative degradation of lipids (lipid peroxidation), phospholipid hydroperoxide glutathione peroxidase (GPX4) expression and its regulating redox factors NRF2, KEAP1 and HMOX1.

2. Materials and methods

2.1. Cells lines and treatment with plasma-treated water

We used the human adenocarcinoma pancreatic cancer cell line BxPC-3 (ATCC® CRL-1678) and the ductal human carcinoma cell line (PANC-1, ATCC® CRL-1469). We treated deionized water with physical plasma, yielding so-called plasma-treated water (PTW), which we applied to the cell lines, as an alternative to direct plasma treatment, with larger applicability

for tumors inside the body. The PTW was prepared using the kINPen® IND plasma jet (INP Greifswald/neoplas tools GmbH, Greifswald, Germany), as described previously [13]. Briefly, plasma was generated with argon gas with a flow rate of 3 LPM, and we kept a 10 mm distance between the nozzle of the plasma jet device and the liquid surface. The plasma irradiation time onto the liquid was 10 min for all treatments (**Fig. S1**). In our previous study we quantified the level of H₂O₂ and NO₂⁻ in PTW at the same conditions, where we detected H₂O₂/NO₂⁻ concentrations of resp. 1400 μM/125 μM inside the PTW [19]

2.2. Analysis of cell cytotoxicity and cell death

The cytotoxicity of PTW was evaluated on two pancreatic cancer cell lines: BxPC-3 and PANC-1. BxPC-3 cells were cultured in RPMI supplemented with 10% FBS, 1% non-essential amino acids, 1% glutamine, 1% penicillin (100 IU/ml) and streptomycin (100 mg/ml) (ThermoFisher Scientific, Massachusetts, USA), whereas the PANC-1 cells were maintained in DMEM supplemented with 10% FBS, 1% non-essential amino acids, 1% glutamine, 1% penicillin (100 IU/ml) and streptomycin (100 mg/ml), all from Gibco™ (ThermoFisher Scientific, Massachusetts, USA). Both cell cultures were maintained in a 5% CO₂ environment at 37 °C, and 95% relative humidity. The cells were grown in 75 cm² tissue culture flasks until they reached confluence and 2x10⁵ cells/ well were seeded into a 24-well plate to grow in complete media. After 24 hours, the culture medium was replaced by different percentages of PTW, i.e., 20, 10, and 5%, or with the ferroptosis inducer Erastin (Era) (Sigma-Aldrich, Missouri, USA), at concentrations of 10, 5, 2.5, or 1.2 μM, for another 24 hours. The cell viability was determined by MTT (3- [4,5- dimethylthiazol-2yl]-2,5-diphenyltetrazolium bromide) assay (Sigma-Aldrich, Missouri, USA) according to the manufacturer's instructions. The ability of PTW to induce iron-dependent cell death was monitored with the CellTox™ Green Cytotoxicity Assay kit (Promega, Wisconsin, USA) according to the manufacturer's protocol. For this approach, BxPC-3 and PANC-1 cells were stimulated during different time

intervals (2, 4, 6 and 8 hours) with 10% PTW alone or in combination with 2 mM of the ROS scavenging agent NAC (N-Acetyl-L-cysteine), the iron chelators, ferroptosis inhibitors Ferrostatin 1 (Fer-1) (Sigma-Aldrich, Missouri, USA), Deferoxamine (DFO) purchased from Abcam (Cambridge, UK), the necroptosis inhibitor Necrostatin-1 (Nec-1) (Sigma-Aldrich, Missouri, USA) and the caspase inhibitor zVAD (Bachem, N-1510) used at 10 μ M.

2.3. Release of Reactive Oxygen Species (ROS)

PTW at 10% was the optimal concentration selected for further molecular studies, based on IC₅₀ values obtained in the cell viability assay. To measure the release of ROS, both, BxPC-3 and PANC-1 cells were seeded at 1×10^4 cells/ml in a 96 well plate and stimulated for 12 hours with 10% PTW, with or without the presence of 2 mM of the ROS inhibitor N-Acetyl-L-cysteine (NAC) obtained from Sigma-Aldrich (Missouri, USA). Subsequently, 50 μ M of CellROX Green Reagent (ThermoFisher Scientific, Massachusetts, USA) was added and the fluorescence intensities were quantified in real time with an IncuCyte ZOOM[®] system (Essen Bioscience, Michigan, USA).

2.4. Intracellular Fe^{2+} analysis

The cellular Fe^{2+} concentration in PANC-1 and BxPC-3 cell lysates was assessed using an iron colorimetric assay kit from Biovision (K390, Milpitas, California, USA) according to the manufacturer instructions. In this assay, ferric carrier proteins dissociate ferric ions into solution in the presence of acid buffer. After reduction to the ferrous form (Fe^{2+}), iron reacts with Ferene S to produce a stable colored complex. The Fe^{2+} concentration was determined by plotting the standard curve (0 to 10 nmol of iron).

2.5. Staining of intracellular reactive oxygen species (ROS) & Lipid Peroxidation

For fluorescence imaging of the intracellular release of ROS, cells were first seeded (1×10^5 cells/ml) on cover glasses and incubated at 37°C, 5 % CO₂ for 24 hours. Subsequently, the slides were incubated with 10% PTW alone or in combination with 2 mM NAC and 0.5 μ M

of the ferroptosis inhibitor Fer-1 for 3 hours. Subsequently, ROS intracellular production was detected after incubating for 30 minutes with 50 μM of cell-permeant reagent: 2', 7'-dichlorofluorescein diacetates (H2DCFDA, ThermoFisher Scientific, Massachusetts, USA), and 10 μM Image-iT™ Lipid Peroxidation Kit, for live cell analysis (ThermoFisher scientific, Massachusetts, USA). The following step was a 20 min fixation in 4% paraformaldehyde (in PBS) and permeabilization in cytoskeleton buffer (pH 6.8, 50 mM NaCl, 150 Mm sucrose, 3 mM MgCl₂, 50 mM Trizma-base, 0.5% Triton X-100). After permeabilization, the slides were washed three times with 1X PBS and mounted with ProLong®Gold Antifade Mountant with DAPI (ThermoFisher scientific, Massachusetts, USA). Images were obtained with a Zeiss AxioImager Z1 microscope (Carl Zeiss, Göttingen, Germany) equipped with an AxioCam MR ver.3.0 using a 40X magnification and filters for green fluorescent (GFP), red (Texas Red) and blue fluorescent (DAPI) channels.

2.6. Quantification of lipid peroxidation by flow cytometry

Flow cytometry was used for a quantification of lipid peroxidation, using the same experimental set-up described above. The treated/untreated cells were incubated with 10 μM of Image-iT for 30 min, then harvested by trypsinization, and washed twice with PBS. Next, the cells were resuspended in PBS to detect the fluorescence intensity by flow cytometry (Attune NxT Flow Cytometer, Brussels, Belgium).

2.7. Quantification of malondialdehyde (MDA)

To evaluate the formation of the lipid peroxidation product MDA, the BCxP-3 and PANC-1 cells were cultured (1×10^5 cells/ ml) at 37°C, 5 % CO₂ for 24 hours. Then, slides were incubated with 10% PTW or 0.5 μM of lipid peroxidation inducer Fer-1 for 3 hours. Subsequently, the concentrations of MDA were quantified using the Lipid Peroxidation (MDA) Assay Kit (Sigma-Aldrich, USA) according to the manufacturer's instructions.

2.8. Quantitative Real Time PCR for oxidative stress related genes

For gene expression analysis, cellular total RNA was isolated using the Purelink™ RNA Mini kit (Ambion, Texas, USA) in combination with the RQ1 Rnase-Free DNase (Promega, Madison, USA) following the producer's instructions. The generated RNA was quantified using an Epoch Microplate Spectrophotometer (BioTek, Vermont, USA) and 2 µg was used to generate cDNA using SuperScript® II Reverse Transcriptase kit (ThermoFisher, Massachusetts, USA). PCR reactions were performed in a StepOnePlus™ Real Time PCR system (Applied Biosystems, California, USA) containing 10 ng cDNA (total RNA equivalent), 1X SYBR Green I (ThermoFisher Scientific, Massachusetts, USA) and 150 nM of the following primer sets: *HMOX1*-Fwd: 5'-CCAGCGG-GCCAGCAACAAAGTGC-3', *HMOX1*-Reverse: 5'-AAGCCTTCAGTGC-CCACGGTAAGG-3' (RefSeq: NM_002133.3); *NRF2*-Forward: 5'-TTCCCGGTCACATCGAGAG-3', *NRF2*-Reverse: 5'-TCCTGTTGCATACCGTCTAAACT-3' (RefSeq: NM_006164.5), *KEAP1*-Forward: 5'-TGCTAACCTCTATACATGCAACT-3', *KEAP1*-Reverse: 5'-GCAACGGT-CAAAGAAGACT-3' (RefSeq: NM_012289.4); *GAPDH*-Forward: 5'-GGAAGCATAAG-AACATCGGAACTG-3', *GAPDH*-Reverse: 5'-GGAGTGGGTGTCGCTGTTG-3' (RefSeq: NM_002046.7); *HPRT1*-Forward: 5'-TGAC-ACTGGCAAACAATGCA-3' or *HPRT1*-Reverse: 5'-GGTCCTTTTCACCAGCAAGCT-3' (RefSeq: NM_000194.3) in a total volume of 50 µl. The amplification protocol consisted of a denaturation step at 95 °C for 10 min, followed by 40 cycles at 95 °C for 15 sec and 60 °C for 1 min. Finally, melting curves of the amplicons were generated by increasing thermal cycling temperature for 1°C every 5 sec from 60°C to 95°C. The relative gene expression was calculated using the comparative quantitative PCR data analysis software qbase+ (version 3.0, Biogazelle, Zwijnaarde, Belgium). As reference genes for normalization, we selected *GAPDH* and *HPRT1* after a selection based on expression stability performed in the GeNorm algorithm also available in the qBase+ software (Biogazelle, Zwijnaarde, Belgium).

2.9. Assessment of Glutathione levels

Glutathione (GSH) levels were measured using the QuantiChrom Glutathione Assay Kit (BioAssay Systems, DIGT-250) according to the manufacturer's protocol. Briefly, the cells were seeded at 2×10^5 cells/ml in a 5-cm dish, and after 24 hours in culture, they were treated with 10% PTW for 3 hours with or without the presence of 4 μ M of Fer-1. After stimulation, the cells were collected and centrifuged at 425 g at 4°C for 5 minutes. The cell pellet was resuspended in 1X PBS and lysed by sonication at a frequency of 20 kHz. Subsequently, the lysates were centrifuged at 18,500 g, 4°C for 10 minutes and supernatants were used to determine the GSH concentrations.

2.10. GPX Enzyme Activity Assay

GPX enzyme activity was analyzed with a commercialized colorimetric BioVision Glutathione Peroxidase Activity Assay Kit (BioVision, Milpitas, CA). In short, PANC-1 and BxPC-3 cells after stimulation were centrifuged at 10,000 x g for 15 min at 4 °C in 200 μ L cold GPX assay buffer, and the assay was performed following the kit protocol. One unit of enzymatic activity is defined as 1.0 μ mol of NADPH oxidized to NADP⁺ per minute at 25 °C.

2.11. Western blot analysis

The protein concentrations of GPX4, KEAP1, NRF2 and HMOX1 were determined in the BxPC-3 cells treated, during 3 hours at 37°C and 5% CO₂, with DMEM culture medium or 10% PTW, with or without the presence of 4 μ M Fer-1. After incubation, the cells were detached and the protein content was extracted with RIPA lysis buffer (Cell Technology, Massachusetts, USA), containing proteinase inhibitor (cOmplete™, EDTA-free Protease Inhibitor Cocktail, Sigma-Aldrich, Missouri, USA) plus PhosphataseArrest™ Phosphatase Inhibitor Cocktail (G-Biosciences, Missouri, USA). Subsequently, the cells were centrifuged for 15 minutes at 13200 g at 4°C and the supernatant containing the soluble proteins was stored at -80°C until use. Subsequently, the protein lysates (20 μ g) were mixed with 5X sample buffer (5% SDS, 20 % glycerol, 0.2 % bromophenol-blue, 250 mM DTT, 65 mM Tris HCl) all

purchased from Sigma Aldrich (Missouri, USA), heated for 5 minutes at 95°C and separated in a 12% SDS-PAGE gel. After separation, the proteins were transferred onto a Nitrocellulose Membrane (BioRad, California, USA) during 2 hours at 45 V. Non-specific binding sites were blocked by incubating the membranes with blocking buffer (0.05 % Tween 20, 1x TBS, 5% BSA) for 1 hour at room temperature. The membrane was then incubated overnight at 4°C, with the following primary antibodies: Rabbit anti-Glutathione Peroxidase 4 antibody (Abcam, Cambridge, UK), Rabbit anti-KEAP1 (Proteintech, Manchester, UK), Rabbit anti-HMOX1 antibodies (Cell Signalling Technology, Massachusetts, USA), Rabbit NRF2 (Abcam, Cambridge, UK), and Rabbit anti-alpha actin (Abcam, Cambridge, UK). This step was followed by an incubation with (1:10000) Donkey anti-Rabbit IgG (H+L) Secondary Antibody-HRP (Thermo Fisher Scientific, Massachusetts, USA) for one hour at room temperature. Chemiluminescence detection was performed using the ECL detection kit (Pierce™ ECL Western Blotting Substrate, Thermo Fisher Scientific, Massachusetts, USA) in a ChemiDoc MP system (BioRad, California, USA). Band intensities were analyzed by the imageJ software [21] and normalized against the intensities of α -tubulin.

2.12. Chicken egg chorioallantoic membrane (CAM) assay

Four-day old fertilized chicken eggs were incubated in a horizontal position for 1 day at 37.7 °C and 65% humidity in an egg incubator with automatic turning function (Ova-Easy 100, Brinsea, Veenendaal, The Netherlands). On day 5, the upper pole was disinfected and pierced with a 20G sterile needle (BD) and sealed with medical tape (Leukosilk S, Covamed Farma BVBA, Marke, Belgium). The eggs were incubated in vertical position (turning function off) to promote the relocation of the air cell. On day 7, the egg shell was cut to expose the chicken chorioallantoic membrane (CAM). A 1 × 1 mm filter paper soaked in diethyl ether (Thermo Fisher Scientific, Massachusetts, USA) was briefly applied on a vascularized region of the CAM and a sterile silicone ring (ID = 5 mm, OD = 6 mm) was placed. A pellet of BxPC-

3 cells (2×10^6 cells per egg) was mixed with 15 μL growth reduced factor Matrigel (8.6 mg/mL, Corning, Amsterdam, The Netherlands) and loaded into the ring. The eggs were sealed with Tegaderm (3D) and placed back in the incubator for 4 days. On day 11, the Tegaderm was cut and a sterile plastic ring (ID = 7 mm, OD = 8.5 mm) was placed around the tumor. Subsequently, 100 μl of 10% PTW mixed with PBS and 100 μL of 10% untreated water mixed with PBS were loaded into the ring. The eggs were sealed with Tegaderm and incubated until the end of the experiment. The cytotoxic effect of the treatments was assessed on day 14 when the tumors were excised and weighed in a precision balance (Mettler Toledo, Fisher, Merelbeke, Belgium). All steps outside the incubator were carried out using a heat block (set at 37.7 °C) with a custom-made egg-shaped aluminium adapter.

2.13. Assessment of cell proliferation by Ki67 staining

For immunohistochemistry, tumor sections (5 μm), obtained from the CAM assay, were fixed in 4% paraformaldehyde, embedded in paraffin, cut in 5- μm sections and stained with 1:1 hematoxylin and 0.5% eosin solution for histological analysis. For staining with the cell proliferation marker Ki67, antigen retrieval was performed with citrate buffer (10 mM, pH 6), at 96 °C for 20 min. Sections were permeabilised in 0.1% Tween-20 and blocked with 3% H_2O_2 in PBS (10 min, RT) and 2% BSA (30 min, RT). The slides were then incubated with 1:75 dilution of the mouse Anti-Human Ki-67 Antigen (Clone MIB-1, Agilent, Santa Clara, CA, USA) for 40 min at room temperature, followed by incubation with the secondary antibody Envision Flex HRP, Agilent, (Santa Clara, California, USA) during 30 min at room temperature. Diaminobenzidine was used to visualize positive staining and haematoxylin to counterstain.

2.14. Immunohistochemistry of GPX4 enzyme

Expression of GXP4 was evaluated in sections from the CAM-solid tumors. The slides were first incubated with blocking buffer (10% Goat serum, 1% BSA in PBS) for 20–30 minutes

at room temperature followed by an incubation with 1:1000 dilution of the rabbit- mAb anti- Glutathione peroxidase 4 (ab125066, Abcam, Cambridge, UK), overnight at 4°. Subsequently, the stained slides were washed and incubated with secondary antibody HRP goat anti-rabbit IgG, (Abcam, Cambridge, UK), used at a dilution of 1:500. All sections were subsequently imaged with a Zeiss AxioImager Z1 microscope (Carl Zeiss, Göttingen, Germany) equipped with an AxioCam MR ver.3.0 (Carl Zeiss, Göttingen, Germany).

2.15 Immunofluorescence of HMOX1

We performed immunofluorescence assays to evaluate the expression of Heme Oxygenase 1 (HMOX1) in sections from the CAM-solid tumors. After antigen retrieval, the slides were first incubated with blocking buffer, i.e., 5% BSA in PBS at RT, followed by an incubation with 1:100 dilution of the Anti-Heme Oxygenase 1 (ab68477, Abcam, Cambridge, UK) overnight at 4°C. Subsequently, the stained slides were washed (with 0.05% Triton X-100) and incubated with secondary antibody Alexa fluor 488 (1:1000; cat. no. ab150077, Abcam), at RT for 1 hour. DAPI was used for nuclear counterstain. All sections were subsequently imaged with a Zeiss AxioImager Z1 microscope (Carl Zeiss, Göttingen, Germany) equipped with an AxioCam MR ver.3.0 (Carl Zeiss, Göttingen, Germany).

2.16 Serine/Threonine (STK) Kinase activity profiling

Serine/Threonine kinase activity was assayed using the PamGene array technology according to the manufacturer's instructions (PamGene International BV, 's-Hertogenbosch, Netherlands). Briefly, BxPC-3 pancreatic cancer cells were cultured with 10% PTW at 37°C, 5% CO₂ for 3 hours. Cell pellets were washed twice with cold 1X PBS and lysed with lysis buffer (1:100) dilution of Halt Phosphatase Inhibitor Cocktail and Halt Protease Inhibitor Cocktail EDTA free in M-PER Mammalian Extraction Buffer (ThermoFisher Scientific, Massachusetts, USA). Lysates were then incubated on ice for 15 min and centrifuged for 15 minutes at 16000 g at 4°C. Supernatants were collected and stored in separate aliquots at -80°C

until use. The protein concentration was quantified using the Pierce BCA Protein Assay Kit (ThermoFisher Scientific, MA, USA).

To determine the kinase activity, PamChip arrays containing 144 immobilized peptides were blocked with 2% BSA, followed by several washing steps. Subsequently, reaction mixes containing 0.5 µg of protein lysate, 1X PK buffer, 1X BSA solution, 0.01 M of STK antibody mix and 0.4 mM of ATP in a final volume of 40 µl were loaded onto the arrays and incubated in the microarray system PamStation® 12 instrument (PamGene International, Den Bosch, Netherlands) following the manufacturer's protocol. Subsequently, peptide phosphorylation intensities were detected by adding 1X Antibody buffer and a secondary STK antibody labelled with FITC. Images were acquired using the CCD camera in the PamStation®12 and processed using the Bionavigator software (PamGene International, Den Bosch, Netherlands). Peptide intensity data were log₂ transformed and differences in phosphorylation between PTW-treated and control cultures were determined using a non-parametric t-test.

To identify potentially activated or inhibited kinases we used the STK Upstream Kinase analysis PamApp from the Bionavigator Software. The analysis is based on “*in silico* predictions” for the upstream kinases of phosphorylation sites in the human proteome that are retrieved from the phosphoNET database [22]. In short, a prediction algorithm is derived from known interactions between kinases and phosphorylation sites and used to predict the strength of undocumented interactions. This app uses Phosphosite PLUS, Phospho.elm, UniPROT, Reactome, Kinexus (PhosphoNet) and STRING databases (<https://string-db.org/>) to map putative kinases upstream of the phospho-peptides (a kinase can have multiple possible phosphosites, and a single site can be phosphorylated by different kinases) and to show kinase network interactions. For each set of peptides mapped to a specific kinase, a “difference statistics” is calculated (normalized kinase statistics) representing the differences in phosphorylation between the two experimental groups.

2.17. Molecular dynamics simulations of GPX4 enzyme

We performed molecular dynamics (MD) simulations to elucidate the stability of native and oxidized GPX4 at the molecular level and to determine the underlying mechanisms of physical plasma induced ferroptotic cell death. Simulations were carried out using the GROMACS [23] program package (version 5.1.2), applying the GROMOS 54a7 force field [24]. The coordinate file (i.e., initial structure) of the human GPX4 was obtained from the Protein Data Bank (PDB ID: 2OBI) [25].

GPX4 was placed in a triclinic box, spacing the atoms at least 1.5 nm from the boundaries of the simulation box. The box was then filled with water molecules surrounding the GPX4, employing the SPC/E (extended simple point charge) water model and neutralized by Na⁺ and Cl⁻. Periodic boundary conditions were applied in all directions. Prior to the simulation, an energy minimization was performed using the steepest descent integration method. Subsequently, the system was equilibrated for 200 ps of the NVT ensemble (constant number of particles N, volume V, and temperature T). Next, a 500 ns production run was conducted within the NPT ensemble (constant number of particles N, pressure P, and temperature T at 310 K) with periodic boundary conditions. It was verified that the 500 ns production run was sufficient, as the native system reached stability after ~200 ns and it remained stable up to 500ns. The temperature was kept constant by V-rescale thermostat [26], while the pressure was maintained by 1 bar using a Parrinello-Rahman barostat [27]. Electrostatic interactions were calculated using the particle mesh Ewald method and cut-off distances for the calculation of Coulomb and van der Waals interactions were 1.0 nm during the equilibration. Note that multiple simulations were carried out using a different cut-off radius and force fields, but the cut-off radius of 1.0 nm and GROMOS 54a7 force field were found to provide the most reliable description of the native GPX4.

To describe the oxidative stage of the protein in the MD simulations, we constructed different oxidation states (OX1 and OX2) of the human GPX4 protein, by selectively manipulating amino acid residues to get their corresponding oxidation states using the Vienna-PTM web server [28]. The oxidation states were defined as follows: C₄₆ was oxidized to cysteic acid and W₁₃₆ was oxidized to 6-hydroxytryptophan, as previously reported and shown in **Figure 4** [29]. Note that for both oxidized structures (OX1 and OX2) we again repeated the minimization, equilibration and production simulation steps, as mentioned above for the native case. The visualizing tool, PyMOL (Schrodinger, New York, USA) was used for image generation [30].

2.18. Statistical analyses

All experiments were performed in at least three independent biological replicates. Bar graphs are represented as the mean \pm S.D (standard deviation). Two groups were compared using Student's t-test with Welch's correction. Pearson's correlation coefficients were computed with a 95% confidence interval. p-values < 0.05 or $p < 0.01$, or $p < 0.001$ were considered statistically significant and labelled with * or ** or ***, respectively, within the graphs as described in the legends. Graphing and statistical analysis were performed using prism 8 (GraphPad software, San Diego, California, USA).

3. Results and discussion

3.1. PTW induces ferroptotic cell death in pancreatic adenocarcinoma BxPC-3 and PANC-1 cells

One of the main challenges in cancer research is to effectively kill tumor cells while leaving healthy cells intact. Cancer cells often have defects in their cell survival machinery, helping them to escape from apoptotic cell death pathways, which is one of the main causes of therapy resistance [19]. To evaluate the potential therapeutic effect of PTW on chemoresistant

pancreatic adenocarcinoma BxPC-3 and PANC-1 cancer cells, we measured changes in cell viability and cell death by the MTT and CellTox™ Green cytotoxicity assays, respectively. The MTT assays showed that 24 hours with PTW decreased cell viability in both cell lines in a dose-dependent manner at concentrations of 5%, 10% and 20% PTW (**Fig. 1A**).

Furthermore, since PTW is a known inducer of oxidative stress which can promote non-apoptotic ferroptotic cell death [31], we also evaluated sensitivity of pancreatic cancer cells to the ferroptosis inducing chemical Erastin (Era). Similar to PTW treatment, Era also reduced cell viability in a dose-dependent manner with a similar efficacy in a concentration range of 2.5-10 μ M (**Fig. 1A**). Upon comparing both dose responses, the BxPC-3 cells revealed similar sensitivity to PTW or erastin treatment, reaching IC₅₀ values upon 10% PTW or 5 μ M Era treatment, respectively (**Fig. 1A and B**). Similar results were obtained for the PANC-1 pancreatic cancer cells (**Fig. 1 A and B**)

To confirm the biochemical involvement of ferroptosis in PTW-induced cell death, we further compared single or combination treatments of PTW with the ferroptosis inducer agent Erastin (Era), ROS scavenging agent NAC (N-Acetyl-L-cysteine), the necrosis inhibitor Necrostatin-1 (Nec-1), the ferroptosis inhibitor Ferrostatin (Fer-1), the iron chelator Deferoxamine (DFO) and the general caspase inhibitor N-Benzyloxycarbonyl-Val-Ala-Asp(O-Me) fluoromethyl ketone (zVAD). As shown in **Figure 1B, S2A and S2B**, Erastin (4 μ M) and 10% PTW treatment alone showed intermediate cytotoxic activity after 8h (approx. 40% cell death, close to IC₅₀ values) in both cell lines. Interestingly, combination treatment of PTW and Era showed additive toxicity, up to 80% of cell death. In contrast, 10% PTW treatment in the presence of NAC, Fer-1 or DFO nearly completely reduced cytotoxicity from 40 to 10% cell death. In contrast, the necroptosis inhibitor Nec-1 and caspase inhibitor zVAD could only partially attenuate PTW-induced cell death (approx. 30% and 25% cell death respectively). Finally, PTW treatment

increased the cellular levels of free Fe^{2+} by more than 2 fold (4.5-5 nM) compared to unstimulated cells, and this effect could not be completely reverted by NAC (**Fig. S2C**).

Altogether, these results suggest that PTW predominantly elicits ferroptosis, and to a lesser extent, necroptosis mediated cell death. This is of importance since pancreatic cancer cells show relative increased ROS levels as compared to non-malignant cells (primarily due to their increased metabolism, oncogene activation, and mitochondrial dysfunction) making them more vulnerable to ferroptosis-specific cancer therapies [6].

3.2. PTW treatment promotes intracellular ROS production and lipid peroxidation in pancreatic adenocarcinoma BxPC-3 and PANC-1 cells, which can be blocked by the ROS scavenger NAC and the ferroptosis inhibitor ferrostatin

Previously, it has been demonstrated that PTW treatment promotes ferroptosis by stimulation of the iron-dependent Fenton reaction to increase intracellular ROS levels and extensive release of malondialdehyde (MDA), one of the final products of polyunsaturated fatty acid peroxidation [10, 32]. Accordingly, we also characterized the potential effect of ROS released upon PTW treatment on the intracellular ROS levels, by measuring changes in cellular fluorescence intensities of CellROX[®]Green Reagent. This cell-permeable compound dye binds to nuclear and mitochondrial DNA and becomes strongly fluorescent upon oxidation. Treatment with 10% PTW resulted in a higher fluorescence intensity when compared to the signal of untreated cells, whereas the ROS scavenger NAC could reverse the effects in BxPC-3 and PANC-1 cell lines (**Fig. 2A and F**). The maximal intensity was significantly increased in treated cells after 4 hours and remained stable for the next 8 hours treatment, as compared to untreated cells.

Similarly, the number of positive fluorescent cells following intracellular staining with the ROS detection probe H2DCFDA, was higher in both (BxPC-3 and PANC-1) cell cultures

with PTW treatment than the number observed in untreated or NAC stimulated cells (**Fig. 2B and G**).

Increasing intracellular RONS levels in response to PTW treatment can further propagate lipid peroxidation and cause lethal damage of cancer cells through ferroptosis [11]. To evaluate the effect of PTW on lipid peroxidation mechanisms in BxPC-3 and PANC-1 cells, we measured the production of malondialdehyde (MDA), which is one of the final products of polyunsaturated fatty acid peroxidation in cells and an established marker of lipid peroxidation stress. As shown in **Figure. 2C**, the intracellular concentrations of MDA in BxPC-3 cells increased more than two-fold after stimulation with 10% PTW, and about two-fold in PANC-1 cells (**Fig. 2 H**), and the effect was reversed by Fer-1 in both cell lines.

Furthermore, lipid peroxidation after PTW treatment alone and in combination with Fer-1, was also quantified using the Image-iT™ Lipid Peroxidation Kit combined with flow cytometry. Lipid peroxidation assay uses the BODIPY® 581/591 C11 lipid peroxidation reporter molecule that shifts its fluorescence from red to green when challenged with oxidizing agents. This probe can penetrate the cellular membrane of living cells and displays a shift in fluorescence (from 590 nm to 510 nm) in the presence of lipid peroxidation products. Using the signal emitted at 510 nm (green color, FITC filter set), we can quantify the amount of lipid peroxidation occurring within the cells. The red fluorescence (emission at 590 nm) represents non-oxidized membrane lipids, the blue color signals represents DAPI (diamidino-2-phenylindole) staining, a blue fluorescent probe that selectively binds double stranded DNA allowing staining of nuclei. The green fluorescence intensity, indicating lipid peroxidation, increased more than three-fold in the BxPC-3 cells and approximately three-fold in the PANC-1 cells after stimulation with 10% PTW. This effect could again be reversed upon Fer-1 treatment in both cell lines (**Fig. 2D and I**).

Finally, the presence of lipid peroxides was also microscopically confirmed by cellular fluorescent staining with the Image-iT (lipid peroxidation) detection reagents. **Figure 2E and J** shows that PTW treatment triggers a strong lipid peroxidation/ fluorescent signal near the cell membranes for both the BxPC-3 and PANC-1 cells. Again, this could be blocked by Fer-1 in both cell lines. Altogether, these results suggest that an increase in intracellular ROS levels promotes ferroptosis through increased lipid peroxidation, which can be inhibited in the presence of Fer-1. Since similar ferroptosis results were obtained in both cell lines, and BxPC-3 and PANC-1 are considered biologically equivalent pancreatic cancer cell lines, subsequent molecular analysis and phospho-kinome profiling studies were pursued only in BxPC-3 cells [33].

3.3 PTW treatment targets the NRF2-KEAP1-HMOX1-GPX4 pathway for ferroptosis sensitization

The nuclear factor E2 related factor 2 (NRF2/NFE2L2) has been proved to play a dual role in (non)-canonical ferroptosis regulation via dynamic changes in KEAP1-HMOX1-GPX4 expression and/or activity [6, 34, 35]. One of the aims of this NRF2 antioxidant response is preventing potential harmful effects of PTW treatment, through the scavenging of the ROS, before they reach concentrations sufficient to induce oxidative lipid peroxidation and DNA damage. However, it operates as a double-edged sword since its constitutive overexpression in pancreatic cancer can also act as a switch for malignancy in cancer, promoting cell proliferation and resistance to cell death processes, such as ferroptosis [34]. Various ferroptosis-related genes are transcriptionally regulated by NRF2, including the antioxidant iron binding heme oxygenase (HMOX)-1, genes for GSH regulation, NADPH regeneration, which are critical determinants of GPX4 activity and iron regulation (including iron export and storage, heme synthesis, and catabolism) [36]. As such, targeting NRF2 overexpression in pancreatic cancer

by PTW treatment may hold promise to reduce pancreatic tumor growth and increase ferroptosis sensitivity.

Accordingly, we measured the transcript and/or protein expression levels of key antioxidant/cytoprotective molecules: KEAP, NRF2, HMOX1, and GPX4 by quantitative real time PCR and Western blot analysis upon PTW treatment. As can be observed from **Figure 3A and B**, PTW treatment abandoned the cytoprotective antioxidant response by decreasing mRNA as well as protein expression of both KEAP1 and NRF2 molecules in BxPC-3 cancer cells, which could be reversed in presence of the ROS inhibitor NAC [37]. Interestingly, at the same time, 3h PTW treatment increased mRNA and protein expression of HMOX1 which was also reversed by NAC as shown in **Figure 3C**. Analysing closely these results it seems a paradox the regulation of Nrf2 and HMOX-1. However, alternative Nrf2 indirect activation mechanisms of HMOX1 have been reported. One of these mechanisms involve chemical oxidative stress induced degradation of the transcription repressor BACH1 [36]. Inactivation of BACH1 has been demonstrated to be sufficient to allow Nrf2 (present in low levels in the nucleus) to bind the HMOX1 promoter and elicit HMOX1 induction [37]. Besides, BACH1 has recently been also identified as another key player of ferroptosis besides NRF2 [38]. Typically, HMOX1 induces a cytoprotective antioxidant response by degrading heme to generate carbon monoxide (CO), biliverdin, and molecular iron under mild oxidative stress conditions. However, when oxidative stress and lipid peroxidation levels increase above the homeostatic stress tolerance, antioxidant cytoprotection may turn into ferroptotic cellular collapse [41]. For example, excessive amounts of HMOX1 trigger sensitization of ferroptosis due to an imbalanced increase of Fe^{2+} levels, insufficient buffering capacity by ferritin and uncontrolled production of hydroxyl radicals via the Fenton reaction [42]. This suggests timely and stochastic NRF2 pathway regulation in response to different cellular levels of ROS [6, 43].

Furthermore, in cancer cells with mutant p53 (such as BxPC-3), downregulation of NRF2 also results in depletion of glutathione levels GSH and suppression of GPX4, which makes cells more vulnerable to ferroptosis [44]. GPX4 inactivation is one of the key features of ferroptosis, which occurs either through a drop in glutathione (GSH) levels and/or by direct oxidative modification of the GPX4 enzyme. Accordingly, we also observed a significant drop in GSH levels and in protein expression of GPX4 (**Fig. 3D**) in the BxPC-3 cells when cultured in the presence of 10% PTW. In contrast, effects were lost in presence of the ferroptosis inhibitor Fer-1, indicating that the excessive lipid peroxidation induced by PTW may be in part due to the inactivation of the GPX4/GSH lipid repair enzyme system, responsible for induction of ferroptotic cell death.

3.4 Molecular dynamics simulations demonstrate oxidative destabilization of the GPX4 catalytic domain

To gain further insight into impairment of GPX4 functions by PTW-induced RONS in response to PTW treatment, we performed molecular dynamics (MD) simulations. This method allows to predict conformational changes in the catalytic active pocket GPX4 upon oxidation. Based on the literature, the active pocket site of GPX4 is located on the solvent accessible surface of the protein, consisting of C₄₆, Q₈₁ and W₁₃₆, also called a catalytic triad (**Fig. 4A**). In the catalytic triad, Q₈₁ and W₁₃₆ are localized at the hydrogen-bond distance to C₄₆, which is a critical determinant of the catalytic activity of GPX4 [25]. Furthermore, it has been shown that GPX4 can be oxidized in multiple oxidation states, which might affect the enzymatic activity of GPX4 [45]. Thus, to determine the effects of oxidation on the arrangements of the catalytic triad upon PTW treatment, three model systems of GPX4 (native, OX1, and OX2) were constructed, where OX1 and OX2 are described as the oxidized structure of GPX4 (**Fig. 4B**). To determine the change in GPX4 structure upon oxidation, we evaluated the root mean square deviation (RMSD) and root mean square fluctuations (RMSF). As shown in **Figure 4C and D**,

the RMSD of the native protein reaches its stable value after 200 ns and remains more or less constant at about 0.24 nm, whereas the RMSDs of the oxidized structures increase with relatively higher fluctuations (especially in the case of OX2 oxidation) compared to the native GPX4. This indicates that the oxidized structures cannot reach the equilibration state during 500 ns of the simulations. Similarly, the physical plasma-derived oxidant effects on the amino acids of GPX4 proteins were analyzed by measuring the time-averaged RMSF values and plotted against residue numbers based on the last 100 ns trajectory data. It is obvious that oxidation of C₄₆ to cysteic acid and W₁₃₆ to 6-hydroxytryptophan will affect the center of mass of the amino acids. Therefore, we calculated the stable alpha carbon (C α) distance between C₄₆ – Q₈₁, C₄₆ – W₁₃₆ and Q₈₁ – W₁₃₆, as shown in **Figure S3A**. In general, the movement and rotation of the side chain of cysteic acid and 6-hydroxytryptophan in the oxidized structures results in a rearrangement of the surrounding amino acids, increasing the C α distances among the catalytic machinery of GPX4. Monitoring the C α distances shows that oxidation of the catalytic residues plays a critical role in the stability of GPX4. Specifically, the C α distances among Q₈₁, cysteic acid and 6-hydroxytryptophan are relatively long for making an H-bond between them. This reduced stability may contribute to a decreased expression of GPX4 observed in our study. The averaged C α distance between the catalytic residue pairs are obtained using the "distance" code implemented in GROMACS. Additionally, we measured the RMSD values of native and oxidized systems only on the catalytic amino acids (**Fig. S3B**) to obtain a deeper insight into the stability of the catalytic machinery of GPX4. The RMSD of the catalytic machinery of GPX4 in the native structure was again found to be more stable in the native case than in the oxidized case.

Next, to experimentally validate the MD simulation results, we measured the cellular changes in enzymatic GPX4 activity upon 10% PTW treatment in BxPC-3 cells. In line with the molecular modeling results, we observed that PTW treatment significantly decreased GPX4

activity, which was attenuated by NAC treatment (**Fig. S3C**). Overall, these MD simulation and experimental results indicate that oxidation of GPX4 leads to a higher dynamic flexibility of catalytic triad, which may reduce the protein stability, in line with our GPX4 expression results shown above (**Fig. 3D**).

3.5 PTW induced kinome activity changes regulate NRF2-KEAP1-HMOX1-GPX4 redox pathway to control autophagy, apoptosis, and ferroptosis cell responses

To further characterize the molecular signalling mechanisms mediating the PTW therapy response in BxPC-3 pancreatic cancer cells, we mapped proteome-wide Ser/Thr kinome activity changes using a phospho-peptidomic approach (Pamchip technology) [46] which translates phosphopeptide fingerprints into cellular kinase network states [46]. Results of this analysis showed that Ser/Thr kinase activities, present in lysates of BxPC-3 cancer cells stimulated for 3 hours with 10% PTW, significantly hyper-phosphorylated 56 consensus Ser/Thr peptide substrates, whereas phosphorylation of 25 other kinase peptide substrates was decreased (**Fig. 5A, 5B and Table S1**). Furthermore, to elucidate which protein kinases are responsible for the changes in phosphorylation observed between the groups, the phospho-peptide fingerprint of significantly hypo/hyperphosphorylated peptides was used as input in the Upstream Kinase application in the BionavigatorTM software algorithm. This bioinformatic analysis combines *in silico* predictions of upstream kinases of consensus phospho-peptide motifs with experimentally determined phospho-peptide intensities. Using a BLAST analysis with the human (phospho)protein reference databases (as explained in the Experimental section), this tool generates a statistical ranking (Fisher's exact test) of activated/inhibited kinases based on scoring penalties of sensitivity and specificity of observed peptide phosphorylation changes in the tested experimental conditions (as shown in **Fig. 5C and Table S2**). This *in silico* analysis predicted partially redundant activity changes of 90 Ser/Thr kinases, based on PTW-induced peptide phosphorylation changes (**Fig. 5D**). More particularly, PTW

treatment predominantly activated the Calcium and Calmodulin-regulated (CAMK) and the AGC kinase groups, with the last one including the cAMP-dependent protein kinase (PKA), the cGMP-dependent protein kinase (PKG) and the protein kinase C (PKC) families (**Fig. 5C and 5D**). In contrast, the 25 peptides showing inhibition of phosphorylation in the plasma-treated cells are mainly substrates of kinases from the CMGC group, which include key kinases, such as the MAPK growth- and stress-response kinases, and the cell cycle CDK (cyclin dependent kinases) (**Fig. 5C and D**).

To further allow biological interpretation of PTW-induced changes in the Ser/Thr kinome activity map, we characterized functional kinase network associations of PTW-activated/inhibited Ser/Thr kinases and the redox regulator molecules NRF2, KEAP1, HMOX1 and GPX4 via the STRING algorithm [47] (**Fig. 6**). Furthermore, KEGG (Kyoto encyclopedia of genes and genomes) pathway enrichment analysis of the kinase signaling network revealed strong enrichment of pancreatic cancer, EGFR tyrosine kinase inhibitor resistance, autophagy, apoptosis and ferroptosis signaling pathways (**Fig. 6 and Table S3**), which are key cell responses to PTW-induced oxidative stress. Interestingly, at the systems kinome level, we identified the mammalian target of rapamycin (mTOR) as a central kinase hub in the PTW-regulated kinase interaction network. (**Fig. 6**, white box). During evolution mTOR has evolved as a key sensor of redox stress homeostasis and lipid energy metabolism [48]. In this respect, mTOR kinase behaves as a systems-level master controller of NRF2-dependent redox pathways towards autophagy, proteostasis or ferroptosis [49]. Altogether, it appears that NRF2/KEAP1/HMOX1/GPX4 protein functions (stability, activity, nuclear translocation) are phospho-regulated by multiple PTW-responsive kinases, which (in)directly modulates sensitivity for autophagy, apoptosis and ferroptosis signalling pathways [41, 50]. As such, final ferroptosis therapy sensitisation by PTW treatment may depend on the systems level integration of multiple Ser/Thr kinase activity changes [50].

3.6 PTW-dependent decrease in GPX4 contributes to ferroptosis specific antitumor effects of BxPC-3 cells grown *ex vivo/in ovo*

Finally, we validated the ferroptosis specific therapeutic effects of PTW treatment on BxPC-3 pancreatic cancer tumor cells grown *ex vivo/in ovo* in the Chorioallantoic Membrane Assay (CAM). After 14 days, tumor sections were analysed macroscopically by H&E and histochemical staining of the proliferation marker Ki67 (**Fig. 7**). The stained tumor sections displayed morphological changes upon PTW treatment, showing cellular shrinking and presence of pyknotic dark small nuclei as a result of chromatin condensation (**Fig. 7A**). In contrast, untreated (control) cells presented a more prominent malignant phenotype with mitotic activity (H&E staining, **Fig. 7A**). In agreement with the H&E staining analysis of tumor specimens, 10% PTW treatment significantly reduced the tumor weight by approx. 74%, as compared to untreated (control) tumors (**Fig. 7B and Fig. 7C**). To assess the proliferative state of cells in the treated tumors, tissue sections were stained for the proliferation marker Ki-67. We observed that tumors exposed to PTW treatment presented the lowest number of Ki-67 positive cells as compared to untreated tumors (**Fig. 7D**). Further, histological sections from PTW-treated tumors showed reduced immunohistochemical staining for the lipid repair enzyme GPX4 when compared to non-treated tumors, in line with reduced GPX4 expression upon PTW treatment (**Fig. 7E**). Finally, to know the contribution of HMOX1 in PTW induced ferroptosis, we also examined histological sections from PTW-treated tumors. We here observed that tumors treated with PTW showed increased expression of HMOX1 as compared to non-treated tumors (**Fig. 7F and Fig. 7G**). These results confirm that the PTW-dependent decrease in GPX4 and increase in HMOX1 expression contribute to ferroptosis specific antitumor effects of BxPC-3 cells grown *ex vivo/in ovo*.

4. Conclusion

In summary, we present a new paradigm in pancreatic cancer treatment for ferroptosis sensitization by PTW treatment (**Fig. 8**). Briefly, plasma generated reactive oxygen and nitrogen species (i.e: hydroxyl ($\cdot\text{OH}$) or alkoxy ($\text{RO}\cdot$) radicals) react with cell membrane poly-unsaturated fatty acids (PUFAs) and produce lipid oxidation products, such as PUFAs-OOH, leading to increased vulnerability for ferroptotic cell death. PTW-generated RONS can be converted to H_2O_2 by superoxide dismutase (SOD) on the cell membrane. When H_2O_2 diffuses into the cell, it subsequently yields highly toxic OH radicals in the presence of reduced iron (Fe^{2+}) through the Fenton reaction, which further increases the intracellular ROS pool. This triggers a systems level mTOR centered kinome response to balance rescue (autophagy) and/or cell death (apoptosis and ferroptosis) signaling pathways. PTW-activated kinases, such as PRKC and GSK3, can trigger NRF2 phosphorylation to regulate its degradation or nuclear translocation [51-53]. Excessive HMOX1 expression/activity induced by PTW-produced ROS, and CAMK4 and AMPK1 kinase activation lead to accumulation of Fe^{2+} and hydroxyl radicals by the Fenton reaction, resulting in ferroptosis sensitization. Further increase of ROS levels will progressively impair the antioxidant defense and lipid repair mechanisms through the NRF2-KEAP1-HMOX1-GPX4 ferroptosis axis. At a critical ROS concentration, PTW treatment will gradually reduce the transcript and protein expression of NRF2 and KEAP1 molecules, resulting in a down-regulation of downstream cytoprotective genes including GPX4 and HMOX1, as well as decreased expression of other pro-oncogenic genes involved in drug and ionizing radiation therapy resistance and cell proliferation. In addition, PTW-triggered ROS can oxidize the GPX4 active pocket, leading to enzyme inactivation and impairment of the GPX4/GSH lipid repair system. Altogether, this will propagate a chain of lipid oxidation products, such as PUFAs-OOH, upon reaction of hydroxyl ($\cdot\text{OH}$) or alkoxy ($\text{RO}\cdot$) radicals with poly-unsaturated fatty acids (PUFAs) [32]. The complete loss of membrane integrity will ultimately result in ferroptotic death of the drug resistant pancreatic cancer cells [35].

Acknowledgments

We gratefully acknowledge the financial support obtained from the Research Foundation Flanders (FWO), Belgium, grant number 12J5617N and Department of Biotechnology (DBT) Ramalingaswami Re-entry Fellowship, India, grant number D.O.NO.BT/HRD/35/02/2006. We are thankful to the Laboratory of Experimental Hematology, for providing the facilities for the experimental and fluorescence microscopy work. The computational work was carried out using the Turing HPC infrastructure at the CalcUA core facility of the University of Antwerp, a division of the Flemish Supercomputer Center VSC, funded by the Hercules Foundation, the Flemish Government (department EWI), Belgium. The Kinome profiling was performed at the Epigenetic Signaling service facility (PPES-UA) funded by the Hercules Foundation and Foundation against cancer Belgium (KOTK 7872).

Conflicts of Interest

The authors declare no conflict of interest.

References

- [1] P. Rawla, T. Sunkara, V. Gaduputi, Epidemiology of Pancreatic Cancer: Global Trends, Etiology and Risk Factors, *World J Oncol* 10(1) (2019) 10-27.
- [2] J.P. Coppé, M. Mori, B. Pan, C. Yau, D.M. Wolf, A. Ruiz-Saenz, D. Brunen, A. Prahallad, P. Cornelissen-Steijger, K. Kemper, C. Posch, C. Wang, C.A. Dreyer, O. Krijgsman, P.R.E. Lee, Z. Chen, D.S. Peeper, M.M. Moasser, R. Bernards, L.J. van 't Veer, Mapping phospho-catalytic dependencies of therapy-resistant tumours reveals actionable vulnerabilities, *Nature cell biology* 21(6) (2019) 778-790.
- [3] E. Kansanen, S.M. Kuosmanen, H. Leinonen, A.-L. Levonen, The KEAP1-NRF2 pathway: mechanisms of activation and dysregulation in cancer, *Redox biology* 1(1) (2013) 45-49.
- [4] S. Gillen, T. Schuster, C. Meyer Zum Büschenfelde, H. Friess, J. Kleeff, Preoperative/neoadjuvant therapy in pancreatic cancer: a systematic review and meta-analysis of response and resection percentages, *PLoS medicine* 7(4) (2010) e1000267.
- [5] C. Holohan, S. Van Schaeybroeck, D.B. Longley, P.G. Johnston, Cancer drug resistance: an evolving paradigm, *Nature reviews. Cancer* 13(10) (2013) 714-26.
- [6] B. Hassannia, P. Vandenabeele, T. Vanden Berghe, Targeting Ferroptosis to Iron Out Cancer, *Cancer cell* 35(6) (2019) 830-849.
- [7] X. Jiang, B.R. Stockwell, M. Conrad, Ferroptosis: mechanisms, biology and role in disease, *Nature Reviews Molecular Cell Biology* (2021) 1-17.
- [8] Y. Shibata, H. Yasui, K. Higashikawa, N. Miyamoto, Y. Kuge, Erastin, a ferroptosis-inducing agent, sensitized cancer cells to X-ray irradiation via glutathione starvation in vitro and in vivo, *PloS one* 14(12) (2019) e0225931.
- [9] A. Privat-Maldonado, A. Schmidt, A. Lin, K.-D. Weltmann, K. Wende, A. Bogaerts, S. Bekeschus, ROS from Physical Plasmas: Redox Chemistry for Biomedical Therapy, *Oxidative Medicine and Cellular Longevity* 2019 (2019) 9062098.
- [10] T. Furuta, L. Shi, S. Toyokuni, Non-thermal plasma as a simple ferroptosis inducer in cancer cells: A possible role of ferritin, *Pathology international* 68(7) (2018) 442-443.
- [11] R. Furuta, N. Kurake, K. Ishikawa, K. Takeda, H. Hashizume, H. Tanaka, H. Kondo, M. Sekine, M. Hori, Intracellular responses to reactive oxygen and nitrogen species, and lipid peroxidation in apoptotic cells cultivated in plasma-activated medium, *Plasma Processes and Polymers* 14(11) (2017) 1700123.
- [12] G.E. Morfill, M.G. Kong, J.L. Zimmermann, FOCUS ON PLASMA MEDICINE, *New Journal of Physics* 11(11) (2009) 115011.
- [13] P. Shaw, N. Kumar, D. Hammerschmid, A. Privat-Maldonado, S. Dewilde, A. Bogaerts, Synergistic effects of melittin and plasma treatment: A promising approach for cancer therapy, *Cancers* 11(8) (2019) 1109.
- [14] L. Magtanong, P. Ko, S. Dixon, Emerging roles for lipids in non-apoptotic cell death, *Cell Death & Differentiation* 23(7) (2016) 1099-1109.
- [15] T. Adachi, S. Nonomura, M. Horiba, T. Hirayama, T. Kamiya, H. Nagasawa, H. Hara, Iron stimulates plasma-activated medium-induced A549 cell injury, *Scientific reports* 6 (2016) 20928.
- [16] O. Lunov, V. Zablotskii, O. Churpita, M. Lunova, M. Jirsa, A. Dejneka, Š. Kubinová, Chemically different non-thermal plasmas target distinct cell death pathways, *Scientific reports* 7(1) (2017) 1-16.

- [17] D. Yan, N. Nourmohammadi, K. Bian, F. Murad, J.H. Sherman, M. Keidar, Stabilizing the cold plasma-stimulated medium by regulating medium's composition, *Sci Rep* 6 (2016) 26016.
- [18] Chen, Zhitong, Xiaoqian Cheng, Li Lin, and Michael Keidar. "Cold atmospheric plasma discharged in water and its potential use in cancer therapy." *Journal of Physics D: Applied Physics* 50, no. 1 (2016): 015208.
- [19] N. Kumar, P. Attri, S. Dewilde, A. Bogaerts, Inactivation of human pancreatic ductal adenocarcinoma with atmospheric plasma treated media and water: A comparative study, *Journal of Physics D: Applied Physics* 51(25) (2018) 255401.
- [20] P. Shaw, N. Kumar, H.S. Kwak, J.H. Park, H.S. Uhm, A. Bogaerts, E.H. Choi, P. Attri, Bacterial inactivation by plasma treated water enhanced by reactive nitrogen species, *Scientific reports* 8(1) (2018) 1-10.
- [21] C. Schneider, W. Rasband, K. Eliceiri, NIH image to ImageJ: 25 years of image analysis. *Nat Meth* 9 (7): 671–675, 2012.
- [22] R. Hilhorst, L. Houkes, A. van den Berg, R. Ruijtenbeek, Peptide microarrays for detailed, high-throughput substrate identification, kinetic characterization, and inhibition studies on protein kinase A, *Analytical biochemistry* 387(2) (2009) 150-161.
- [23] M.J. Abraham, T. Murtola, R. Schulz, S. Pall, J.C. Smith, B. Hess, E. Lindahl, GROMACS: High performance molecular simulations through multi-level parallelism from laptops to supercomputers, *SoftwareX* 1-2 (2015) 19-25.
- [24] N. Schmid, A. Eichenberger, A. Choutko, S. Riniker, M. Winger, A. Mark, W. van Gunsteren, Definition and testing of the GROMOS force-field versions 54A7 and 54B7, *European biophysics journal: EBJ* 40(7) (2011) 843.
- [25] P. Scheerer, A. Borchert, N. Krauss, H. Wessner, C. Gerth, W. Höhne, H. Kuhn, Structural basis for catalytic activity and enzyme polymerization of phospholipid hydroperoxide glutathione peroxidase-4 (GPX4), *Biochemistry* 46(31) (2007) 9041-9049.
- [26] G. Bussi, D. Donadio, M. Parrinello, Canonical sampling through velocity rescaling, *The Journal of chemical physics* 126(1) (2007) 014101.
- [27] M. Parrinello, Polymorphic Transitions in Single Crystals : A New Molecular Dynamics Method, *Journal of Applied Physics* 52(12) (1981) 7812-7190.
- [28] C. Margreitter, D. Petrov, B. Zagrovic, Vienna-PTM web server: a toolkit for MD simulations of protein post-translational modifications, *Nucleic Acids Research* 41(Web Server issue) (2013) W422-6.
- [29] E. Takai, T. Kitamura, J. Kuwabara, S. Ikawa, S. Yoshizawa, K. Shiraki, H. Kawasaki, R. Arakawa, K. Kitano, Chemical modification of amino acids by atmospheric-pressure cold plasma in aqueous solution, *Journal of Physics D: Applied Physics* 47(28) (2014) 285403.
- [30] W. DELANO, The PyMOL Molecular Graphics System, <http://pymol.sourceforge.net> (2004).
- [31] K. Totsuka, T. Ueta, T. Uchida, M.F. Roggia, S. Nakagawa, D.G. Vavvas, M. Honjo, M. Aihara, Oxidative stress induces ferroptotic cell death in retinal pigment epithelial cells, *Experimental Eye Research* 181 (2019) 316-324.
- [32] N. Zarkovic, A. Cipak, M. Jaganjac, S. Borovic, K. Zarkovic, Pathophysiological relevance of aldehydic protein modifications, *Journal of proteomics* 92 (2013) 239-47.
- [33] E.L. Deer, J. González-Hernández, J.D. Coursen, J.E. Shea, J. Ngatia, C.L. Scaife, M.A. Firpo, S.J. Mulvihill, Phenotype and genotype of pancreatic cancer cell lines, *Pancreas* 39(4) (2010) 425.
- [34] M. De La Rojo Vega, E. Chapman, D. Zhang, NRF2 and the Hallmarks of Cancer, *Cancer cell* 34 (2018) 21-43.
- [35] T. Vanden Berghe, B. Hassannia, S. Van Coillie, Ferroptosis: biological rust of lipid membranes, *Antioxidants and Redox Signaling* (2020).

- [36] Z. Fan, A. Wirth, D. Chen, C. Wruck, M. Rauh, M. Buchfelder, N. Savaskan, NRF2-KEAP1 pathway promotes cell proliferation and diminishes ferroptosis, *Oncogenesis* 6(8) (2017) e371-e371.
- [37] H. Huang, Y. Wu, W. Fu, X. Wang, L. Zhou, X. Xu, F. Huang, Y. Wu, Downregulation of KEAP1 contributes to poor prognosis and Axitinib resistance of renal cell carcinoma via upregulation of NRF2 expression, *International journal of molecular medicine* 43(5) (2019) 2044-2054.
- [38] J.F. Reichard, M.A. Sartor, A. Puga, BACH1 is a specific repressor of HMOX1 that is inactivated by arsenite, *Journal of Biological Chemistry* 283(33) (2008) 22363-22370.
- [39] J.F. Reichard, G.T. Motz, A. Puga, Heme oxygenase-1 induction by NRF2 requires inactivation of the transcriptional repressor BACH1, *Nucleic acids research* 35(21) (2007) 7074-7086.
- [40] H. Nishizawa, M. Matsumoto, T. Shindo, D. Saigusa, H. Kato, K. Suzuki, M. Sato, Y. Ishii, H. Shimokawa, K. Igarashi, Ferroptosis is controlled by the coordinated transcriptional regulation of glutathione and labile iron metabolism by the transcription factor BACH1, *Journal of Biological Chemistry* 295(1) (2020) 69-82.
- [41] J.-J. Qin, X.-D. Cheng, J. Zhang, W.-D. Zhang, Dual roles and therapeutic potential of KEAP1-NRF2 pathway in pancreatic cancer: a systematic review, *Cell Communication and Signaling* 17(1) (2019) 121.
- [42] S.-K. Chiang, S.-E. Chen, L.-C. Chang, A Dual Role of Heme Oxygenase-1 in Cancer Cells, *Int J Mol Sci* 20(1) (2018) 39.
- [43] M. Dodson, M.R. de la Vega, A.B. Cholanians, C.J. Schmidlin, E. Chapman, D.D. Zhang, Modulating NRF2 in Disease: Timing Is Everything, *Annual review of pharmacology and toxicology* 59 (2019) 555-575.
- [44] D.S. Liu, C.P. Duong, S. Haupt, K.G. Montgomery, C.M. House, W.J. Azar, H.B. Pearson, O.M. Fisher, M. Read, G.R. Guerra, Inhibiting the system x_C⁻/glutathione axis selectively targets cancers with mutant-p53 accumulation, *Nature communications* 8(1) (2017) 1-14.
- [45] J.K. Eaton, L. Furst, R.A. Ruberto, D. Moosmayer, R.C. Hillig, A. Hilpmann, K. Zimmermann, M.J. Ryan, M. Niehues, V. Badock, Targeting a therapy-resistant cancer cell state using masked electrophiles as GPX4 inhibitors, *bioRxiv* (2018) 376764.
- [46] C.S. Chirumamilla, M.H.U.T. Fazil, C. Perez-Novo, S. Rangarajan, R. de Wijn, P. Ramireddy, N.K. Verma, W.V. Berghe, Profiling activity of cellular kinases in migrating T-cells, *T-Cell Motility*, Springer2019, pp. 99-113.
- [47] D. Szklarczyk, A.L. Gable, D. Lyon, A. Junge, S. Wyder, J. Huerta-Cepas, M. Simonovic, N.T. Doncheva, J.H. Morris, P. Bork, STRING v11: protein-protein association networks with increased coverage, supporting functional discovery in genome-wide experimental datasets, *Nucleic acids research* 47(D1) (2019) D607-D613.
- [48] G.Y. Liu, D.M. Sabatini, mTOR at the nexus of nutrition, growth, ageing and disease, *Nature Reviews Molecular Cell Biology* (2020) 1-21.
- [49] O. Kapuy, D. Papp, T. Vellai, G. Bánhegyi, T. Korcsmáros, Systems-Level Feedbacks of NRF2 Controlling Autophagy upon Oxidative Stress Response, *Antioxidants (Basel)* 7(3) (2018) 39.
- [50] J.H. Kim, G.Y. Park, S.Y. Bang, S.Y. Park, S.K. Bae, Y. Kim, Crocin suppresses LPS-stimulated expression of inducible nitric oxide synthase by upregulation of heme oxygenase-1 via calcium/calmodulin-dependent protein kinase 4, *Mediators of inflammation* 2014 (2014) 728709.
- [51] E. Panieri, L. Saso, Potential applications of NRF2 inhibitors in cancer therapy, *Oxidative medicine and cellular longevity* 2019 (2019).

[52] R. Venè, B. Cardinali, G. Arena, N. Ferrari, R. Benelli, S. Minghelli, A. Poggi, D.M. Noonan, A. Albini, F. Tosetti, Glycogen synthase kinase 3 regulates cell death and survival signaling in tumor cells under redox stress, *Neoplasia* 16(9) (2014) 710-722.

[53] P. Rada, A.I. Rojo, S. Chowdhry, M. McMahon, J.D. Hayes, A. Cuadrado, SCF/ β -TrCP promotes glycogen synthase kinase 3-dependent degradation of the Nrf2 transcription factor in a Keap1-independent manner, *Molecular and cellular biology* 31(6) (2011) 1121-1133.

Figure legend

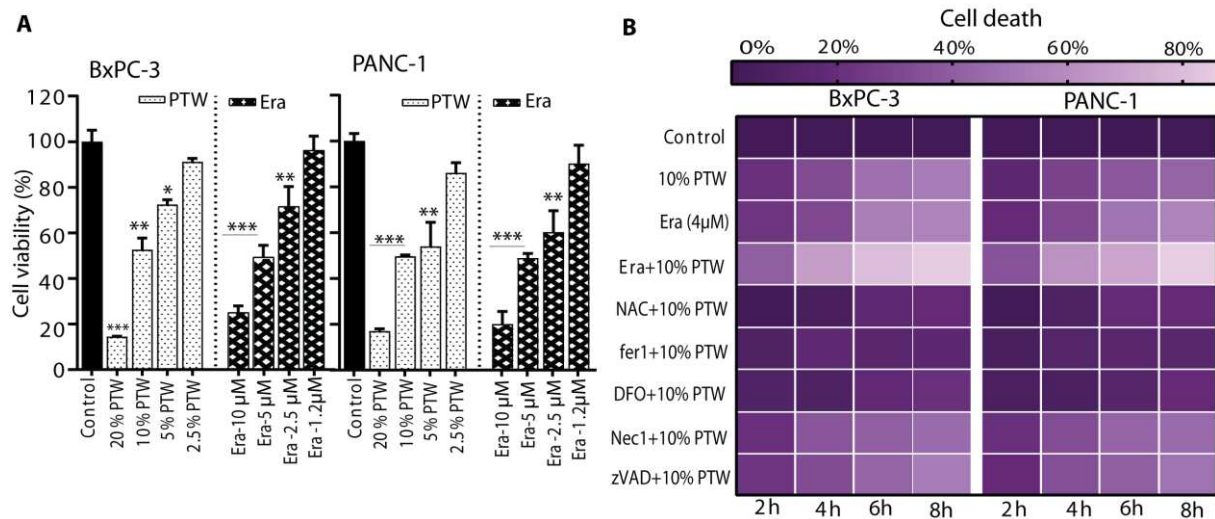


Figure 1. Effect of Plasma-treated water (PTW) on cell viability of BxPC-3 and PANC-1 cells, represented as: (A) percentage of viable cells, as measured by MTT assay, after 24 hours stimulation with different concentrations of PTW and Era. (B) heat map representing percentage of cell death, as measured by the CellTox™ Green Cytotoxicity Assay kit, after incubation with 10% PTW, Era (4 μ M), the ROS scavenging agent NAC (2 mM), the ferroptotic cell death inhibitors Fer-1 and DFO, necroptosis inhibitor Nec-1(50 μ M) and caspase inhibitor zVAD (10 μ M). The results are derived from three independent biological replicates and are shown as mean \pm standard error of the mean (SEM). Statistical analysis was performed using Student's t-test with Welch's correction, * = $p < 0.05$; ** = $p < 0.01$; *** = $p < 0.001$. PTW: Plasma-treated water, Era: Erastin, ROS: Reactive oxygen species, NAC: N-Acetyl-L-cysteine, Fer-1: Ferrostatin, DFO: Deferoxamine, zVAD: benzyloxycarbonyl-Val-Ala-Asp-fluoromethyl ketone (Z-VAD-FMK)

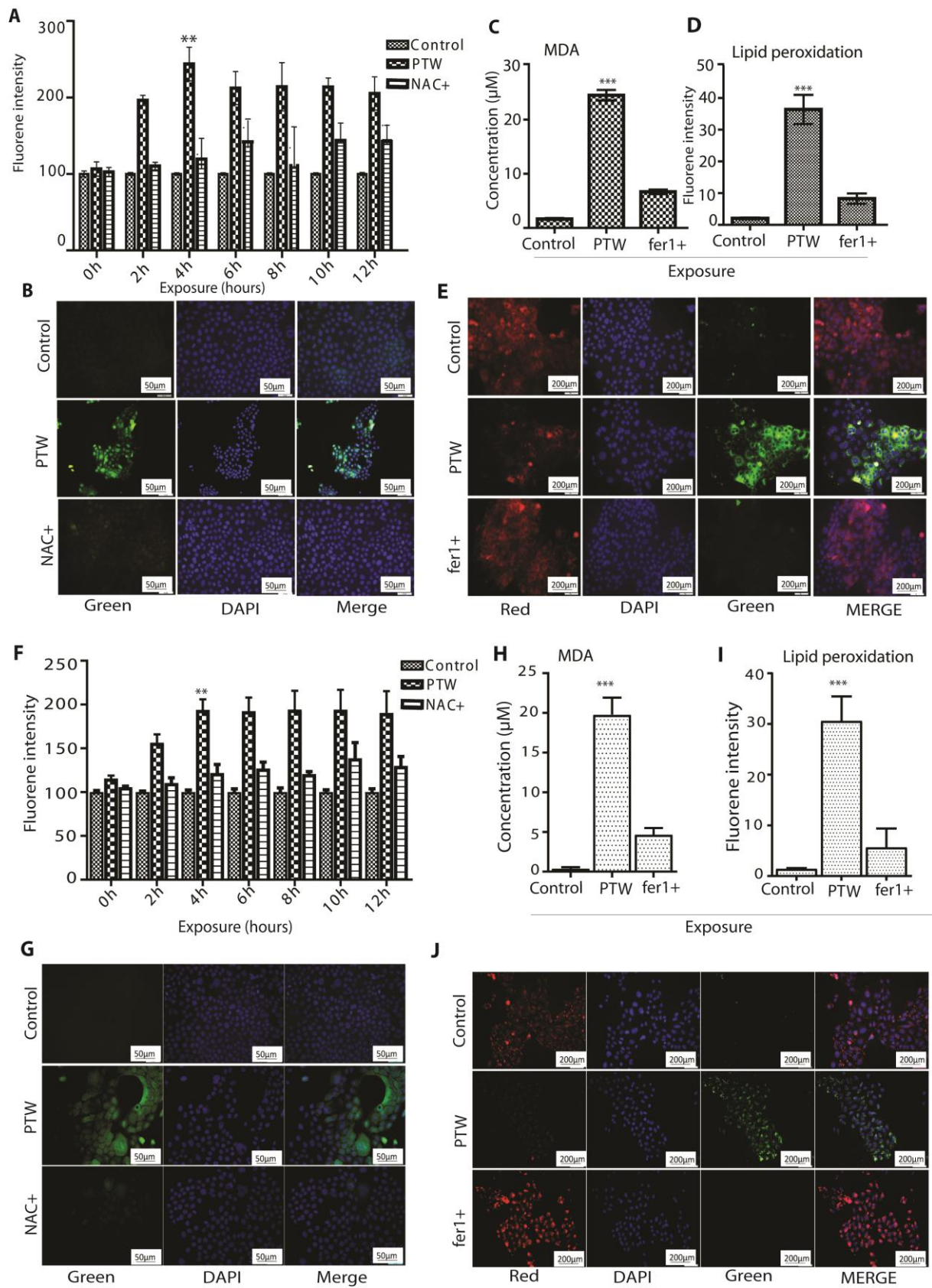


Figure 2. Changes in intracellular ROS content and lipid peroxidation upon treatment with 10% PTW in the presence or absence of NAC in BxPC-3 and PANC-1 cells. (A& F) real-time release as percentage of ROS in PTW-treated versus the percentage in untreated (control) cells measured with the fluorescent Cell[®]Rox green probe. (B&G) fluorescence images of positive BxPC-3 and PANC-1 stained cells with the H2DCFDA fluorescent probe. Green fluorescence represents intracellular ROS, DAPI (blue) represents the nuclear counterstain. Data represent the mean \pm standard error of the mean (SEM) from three independent experiments. Statistical analysis was performed using Student's t-test with Welch's correction (a). ** = $p < 0.01$. ROS: Reactive oxygen species; NAC: N-Acetyl-L-cysteine. (C&,H) Concentrations of malondialdehyde (MDA) after stimulation with 10%-PTW and Fer-1 in BxPC-3 and PANC-1 cells, (D&I) lipid peroxidation products measured using flow cytometry and Image-iT (lipid peroxidation) molecular probe, and (E&J) Fluorescent staining where red fluorescence represents non-oxidized membrane lipids, DAPI (blue) represents the nuclear counterstain and green represents the oxidized membrane lipids in BxPC-3 and PANC-1 cells. Data represent the mean \pm SEM from three independent experiments. Statistical analysis was performed using Student's t-test with Welch's correction (b, c, d). *** = $p < 0.001$. PTW: plasma treated water, NAC: N-Acetyl-L-c

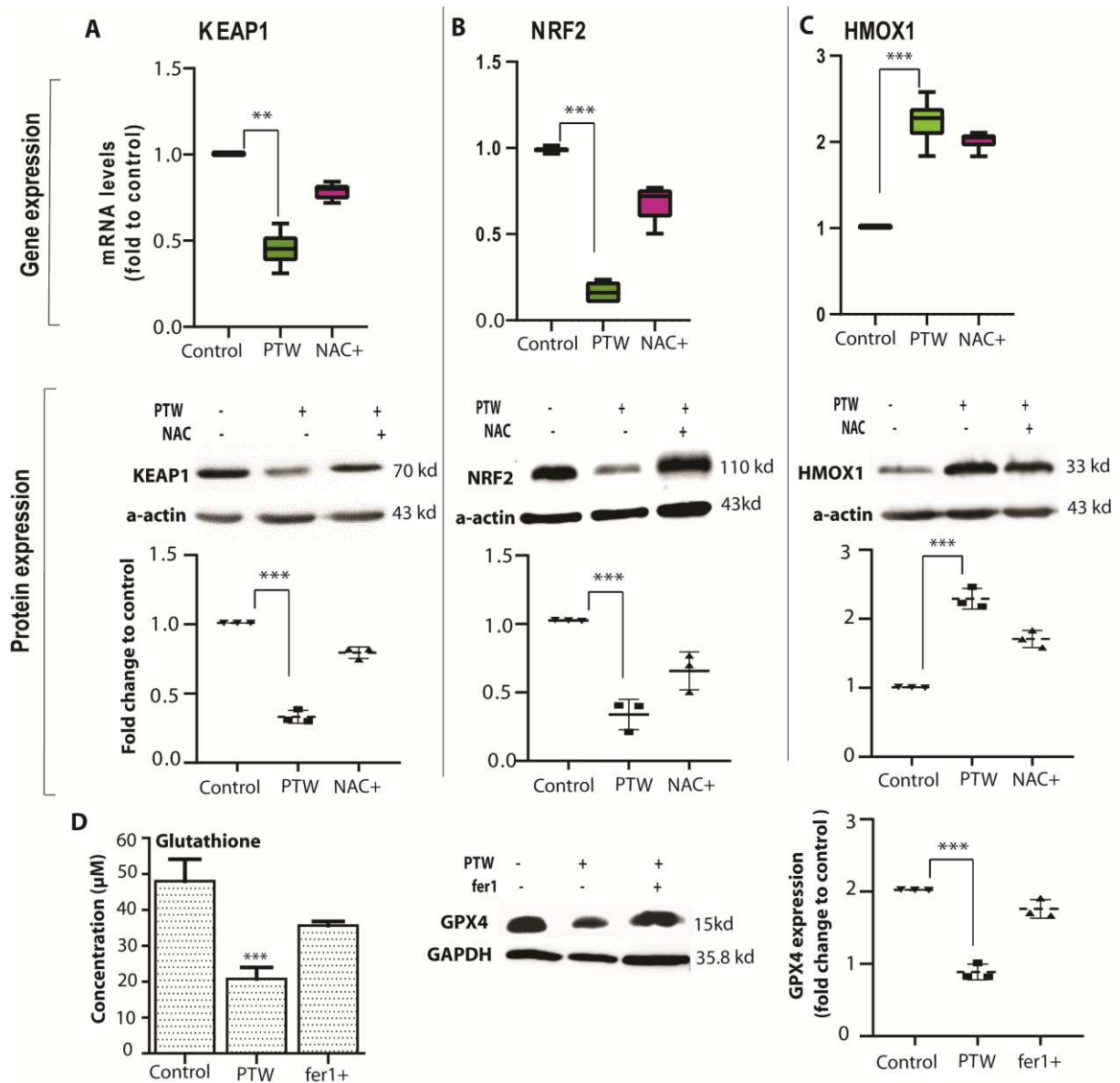
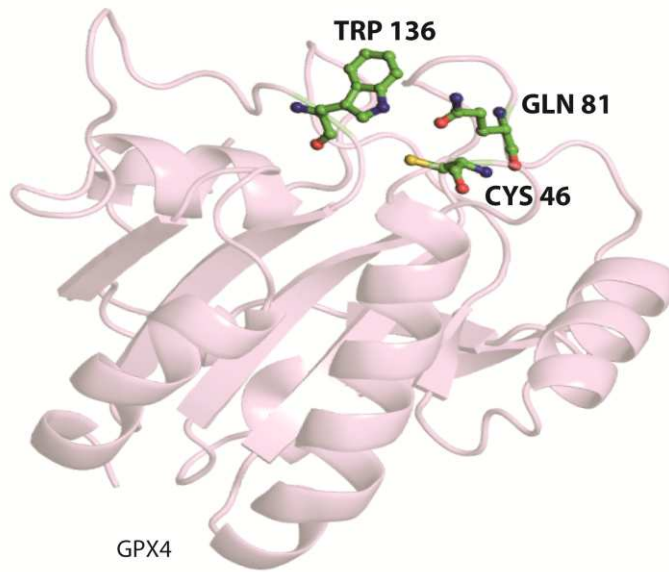
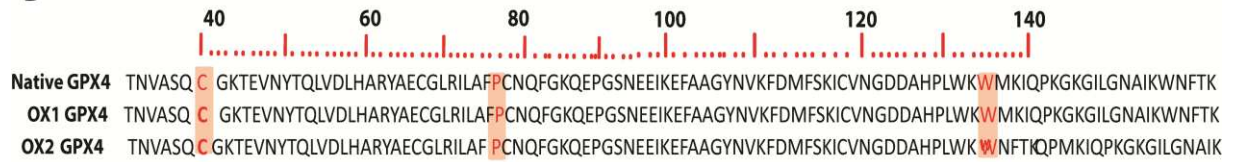


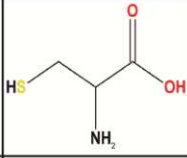
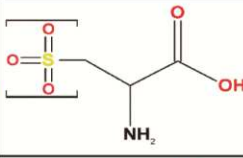
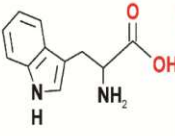

Figure 3. Effect of PTW on the expression of cytoprotective molecules represented as relative normalized fold changes of mRNA expression levels, and protein expression levels (A) KEAP1, (B) HMOX1, and (C) NRF2, as measured by Western blot analysis and bar plot representation of Western signal quantification using image J software (10% PTW or NAC treatment versus untreated cells). (D) Cellular levels of glutathione (GSH) and levels of GPX4 protein expression levels upon 10% PTW treatment in the presence or absence of Fer-1 in BxPC-3 cells. Data represent the mean \pm SEM from three independent experiments. PTW: plasma-treated water, Fer-1: Ferrostatin, NAC: N-Acetyl-L-cysteine.

A

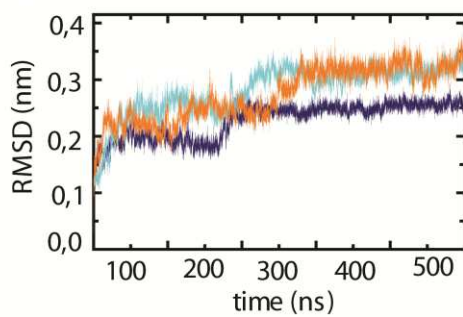


B



Oxidation	Modified AAs in GPX4	Native AA	Oxidized AA
OX1	C46		
OX2	OX1 + W136		

C



D

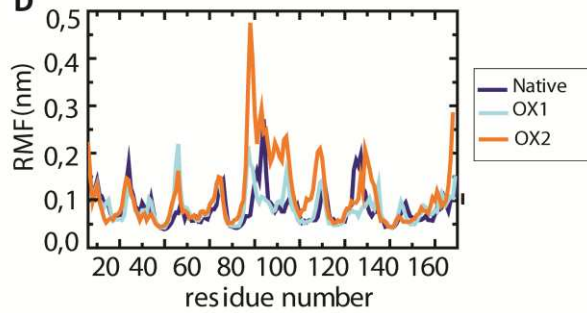
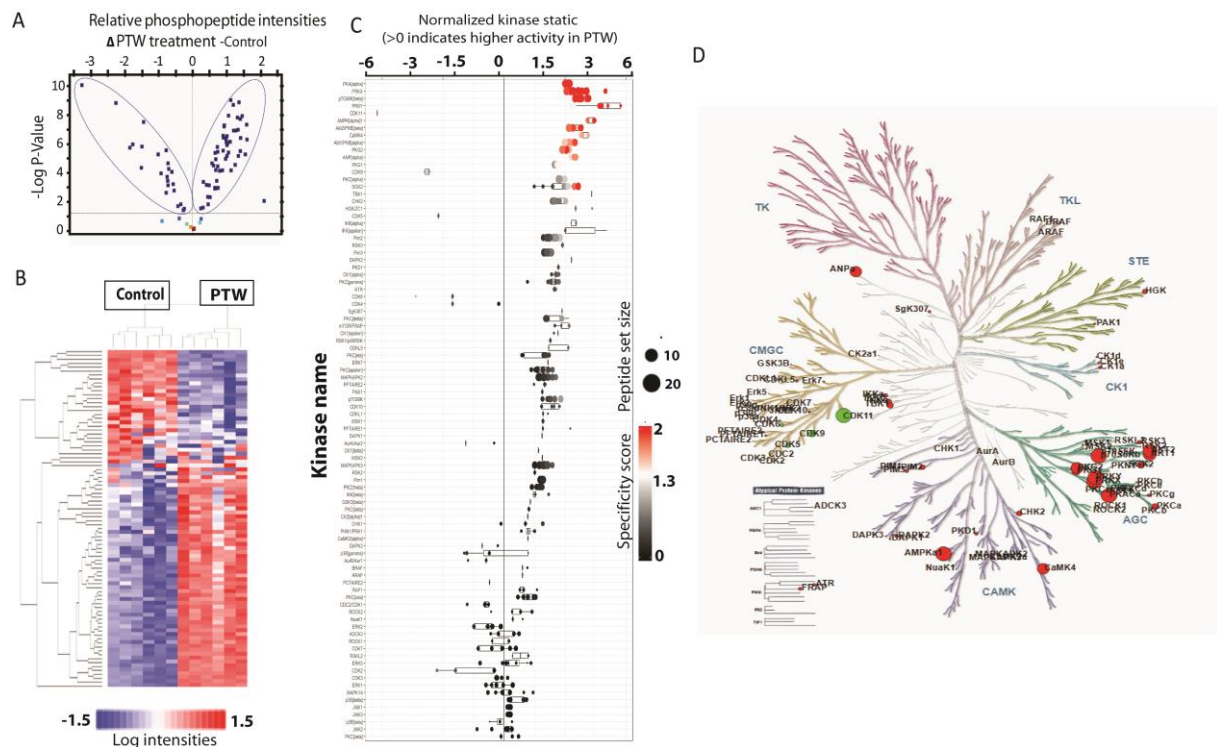


Figure 4. (A, B) Native structure of GPX4 (PDB ID: 2OBI); the catalytic triad is a combination of three amino acid residues: Cys-46, Gln-81, and Trp-136, shown in sticks. (C) RMSD analysis of the backbone of the native, OX1 and OX2 GPX4 structures; (D) RMSF analysis computed on each residue of the GPX4 structures. The table indicates the modified amino acid residues to create the oxidized GPX4 structures.



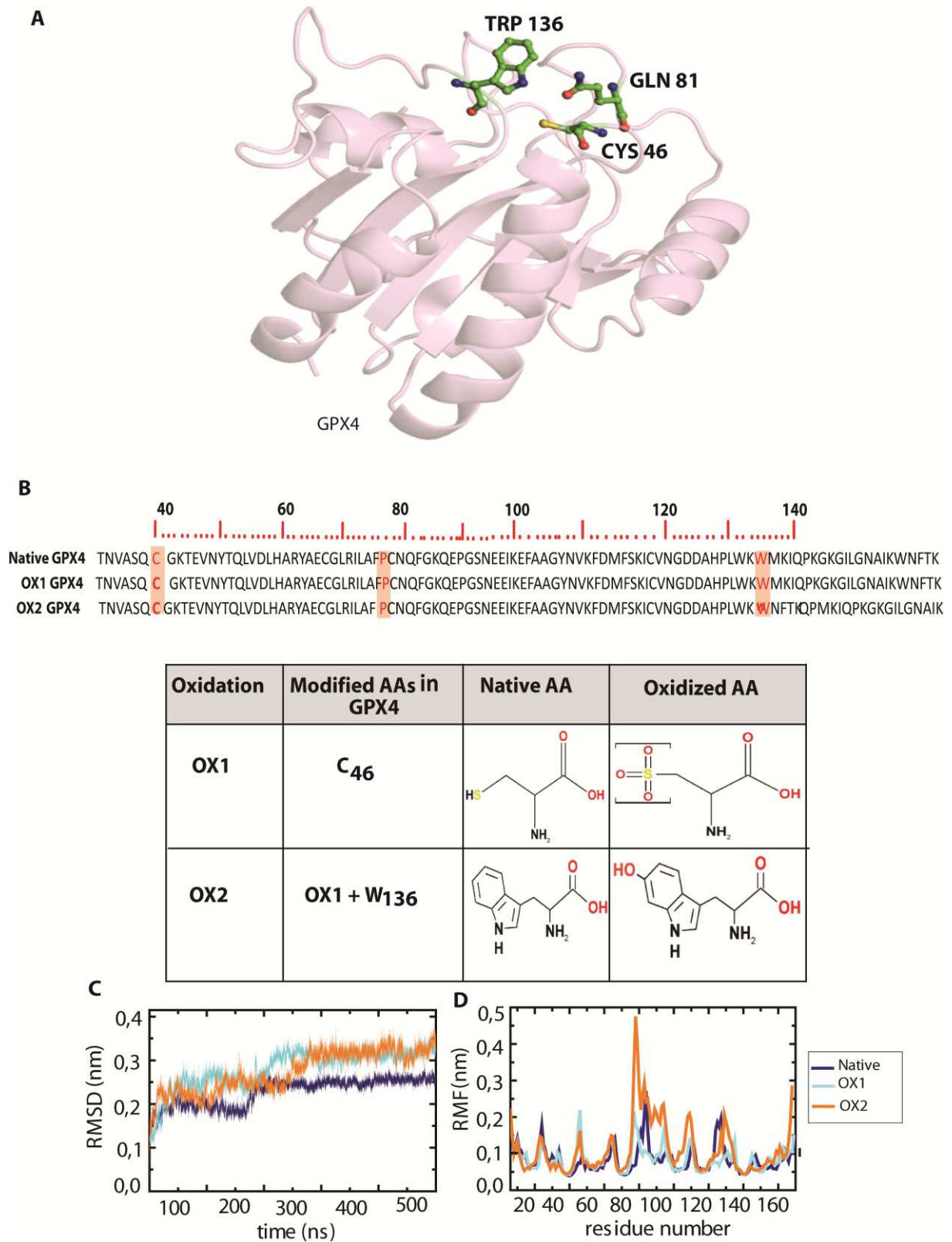
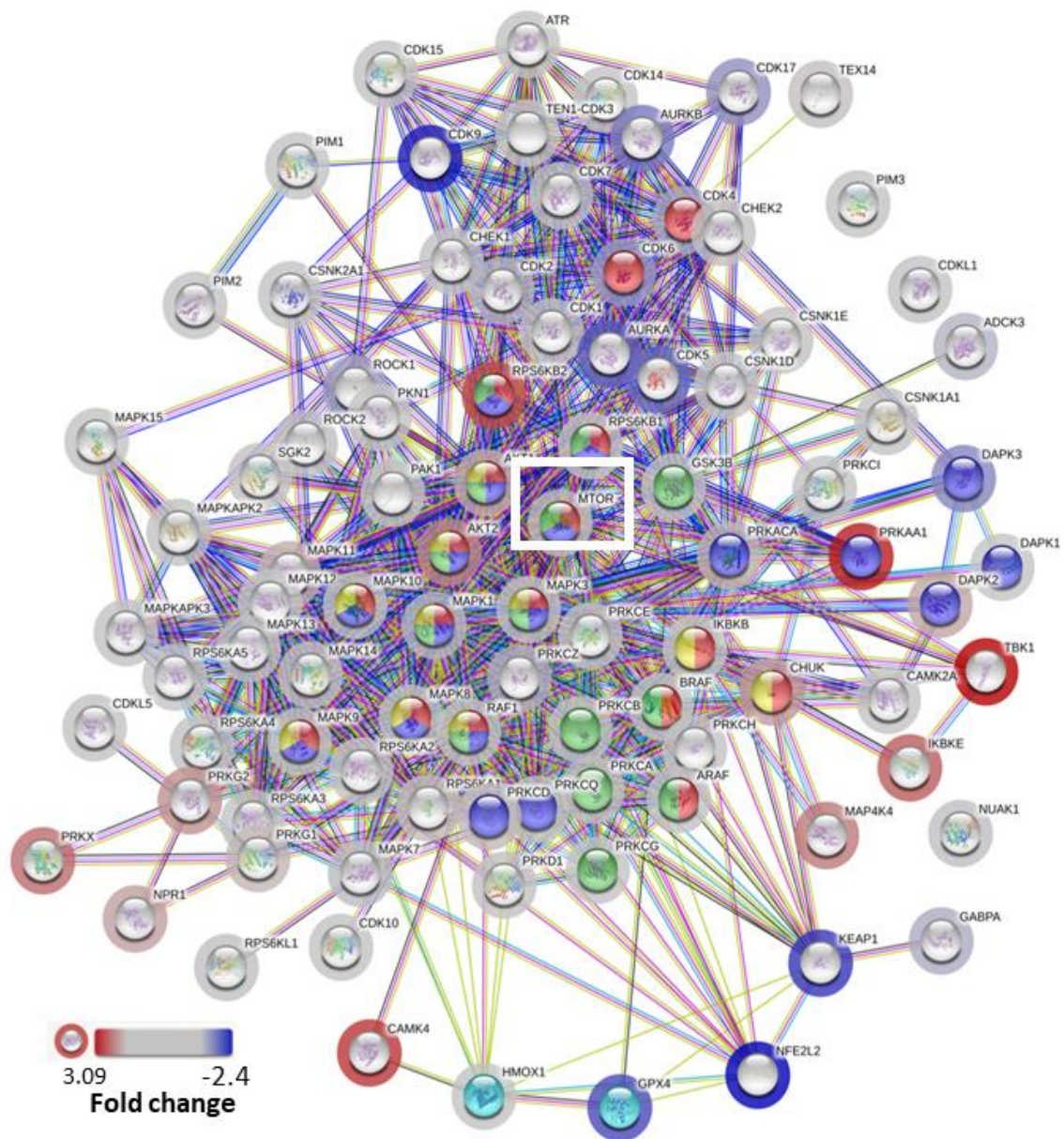


Figure 5. Effect of PTW treatment on the activity of Serine/ Threonine kinases represented as:
(A) scatter plot showing the statistical significant changes in peptide phosphorylation intensities

following PTW-treatment relative to Control cells (B) heatmap clustering the hyperphosphorylated (red) or hypophosphorylated (blue) peptides in Control (untreated) and PTW treated cells, (C) statistical ranking of kinase activity changes according to their final score in the upstream kinase analysis. The right box represents the top ranked kinases, which are most likely the ones playing a key role in the observed experimental differences. The X-axis indicates the values of the normalized kinase statistics. Each point represents an individual analysis with a different rank cut-off for adding upstream kinases for peptides, with the size indicating the size of the peptide set used and the colour of the points indicating the specificity score resulting from the corresponding analysis. (D) View of the kinome tree created by KinMap, showing the kinases with lower activity (green dots) and the hyper-activated kinases (red dots) after stimulation with PTW-treated water of BxPC-3 cells.



Enriched KEGG Pathways

- Pancreatic cancer (FDR: 9.10e-22)
- Autophagy (FDR: 4.99e-20)
- EGFR Tyrosine kinase inhibitor resistance (FDR: 5.04e-17)
- Apoptosis (FDR: 3.2e-09)
- Ferroptosis (FDR: 0.019)

Figure 6. STRING (<https://string-db.org/>) based functional kinase interaction network of hypo- and hyperactivated Ser/Thr kinases after PTW treatment in relation to expression changes of NRF2, KEAP1, HMOX1 and GPX4 proteins. KEGG pathway enrichment analysis of the kinase network shows significant enrichment for biological process related to pancreatic cancer (red), autophagy (purple), EGFR tyrosine kinase inhibitor resistance (green-), apoptosis (yellow) and ferroptosis (turquoise). Kinase dots with multi-color pie-charts are part of multiple biological processes. The colored “halo” around the kinase dots indicates the relative fold-change in activity and/or expression, with red representing relative activation/increase and blue repression/decrease

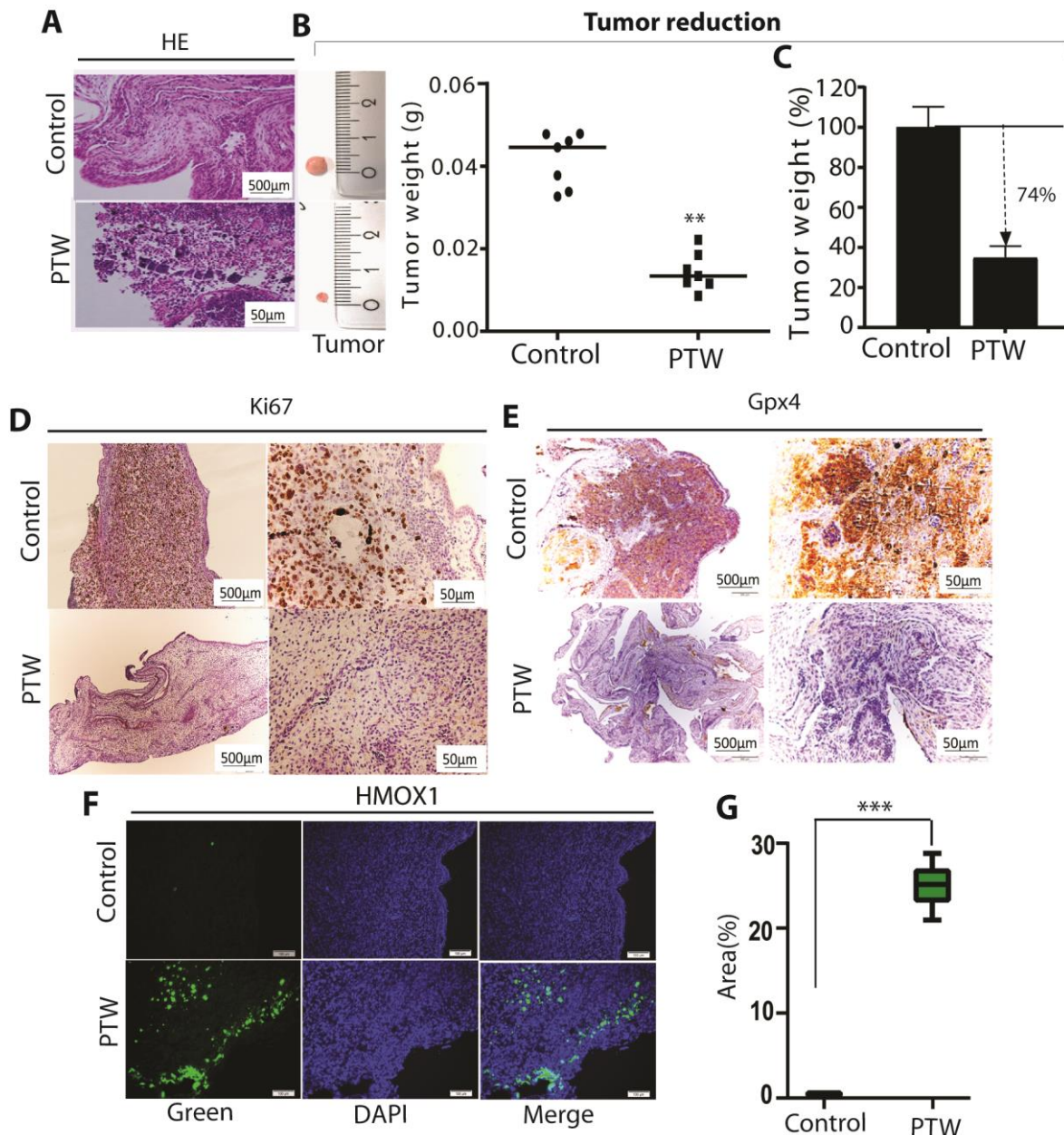


Figure 7. Effect of PTW treatment on tumor weight and cell proliferation in the pancreatic CAM tumor model, showing (A) haematoxylin and eosin staining, (B) weight reduction upon treatments in tumors *in ovo* (each dot represents one tumor). (C) reduction of tumor weight after treatment with 10% PTW (Percentage of tumor weight = weight treated / weight untreated x 100%), (D and E) Histochemical staining showing the reduction of the proliferation marker Ki67 and GPX4 expression in the tumor tissues after treatment with 10% PTW, (F) Representative images of immunofluorescent staining, showing increased HMOX1 expression

in tumor tissues after treatment with 10% PTW. Green represents HMOX1 over-expression, blue (DAPI) represents the nuclear counterstain and merge represents combination of green and DAPI, (G) The staining was scored using ImageJ software (treated versus untreated control setup). Statistical analysis was performed using Student's t-test with Welch's correction (b, c, d). *** = $p < 0.001$

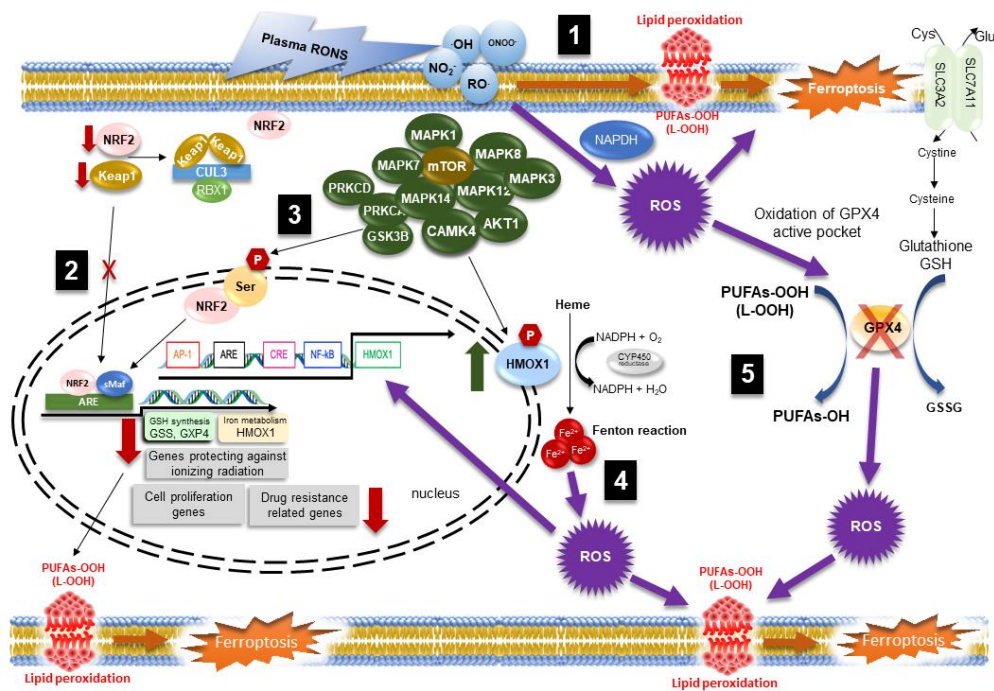
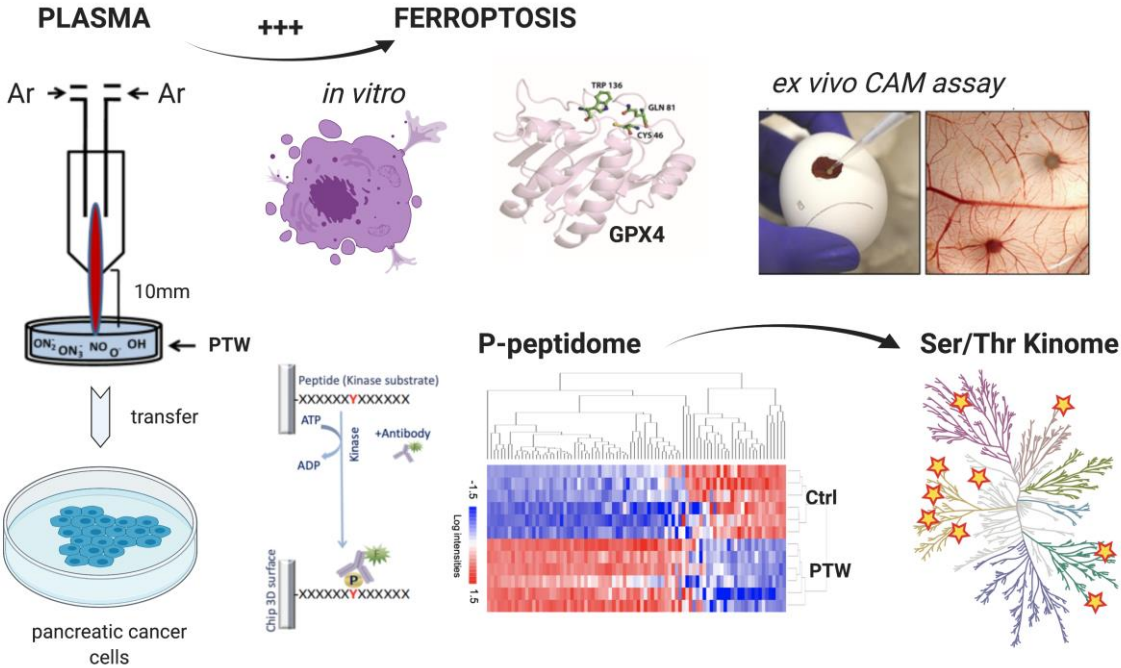


Figure 8. New working hypothesis on ferroptosis sensitization mechanisms by plasma-derived oxidants in pancreatic cells. (1) Plasma generated reactive oxygen and nitrogen species (RONS, i.e: hydroxyl ($\cdot\text{OH}$) or alkoxy ($\text{RO}\cdot$) radicals) react with poly-unsaturated fatty acids (PUFAs) and produce lipid oxidation products, such as PUFAs-OOH, leading to ferroptotic cell death. (2) Plasma treatment reduces the transcript and protein expression of NRF2 and KEAP1 molecules, resulting in suppression of downstream cytoprotective target genes GPX4 and HMOX1, as well as other oncogenic genes involved in therapy resistance and cell proliferation. (3) PTW activates mTOR centered Ser/Thr kinase network, which triggers NRF2 phosphorylation to induce its nuclear translocation. (4) Excessive HMOX1 expression/activity induced by PTW-produced ROS, and CAMK4 and AMPK1 kinase activation lead to

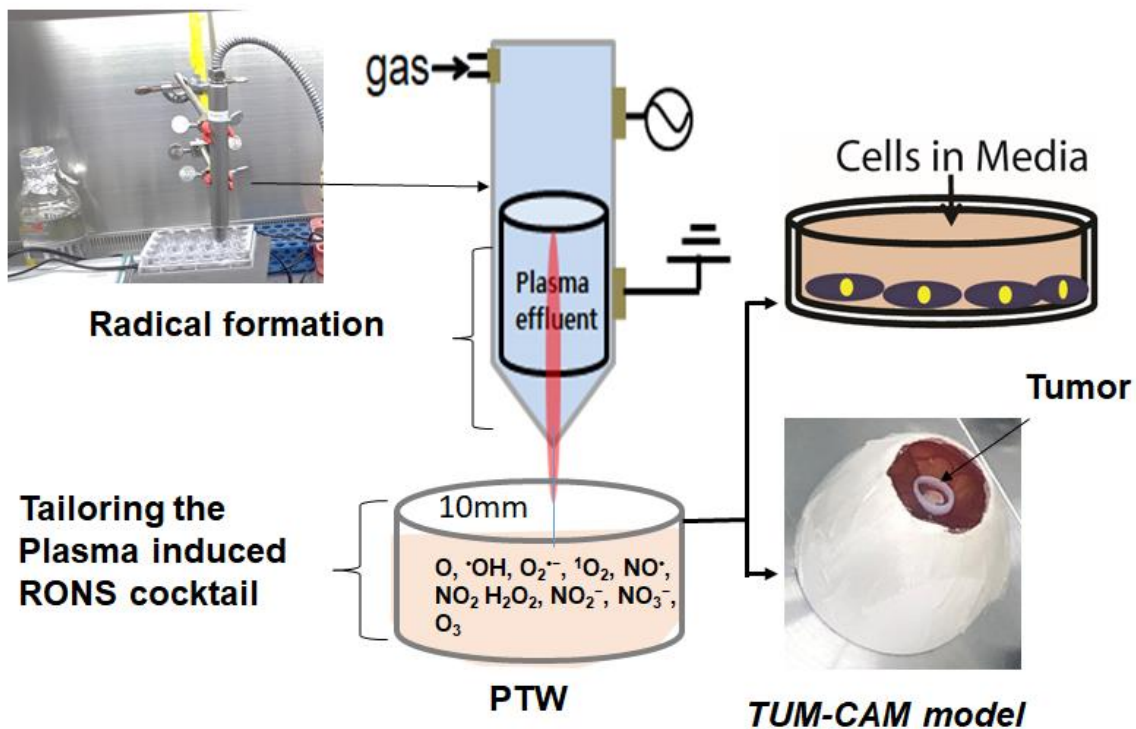
accumulation of Fe²⁺ and hydroxyl radicals by the Fenton reaction, resulting in Ferroptosis. (5)

Plasma-triggered ROS can oxidize the GPX4 active pocket leading to enzyme inactivation.

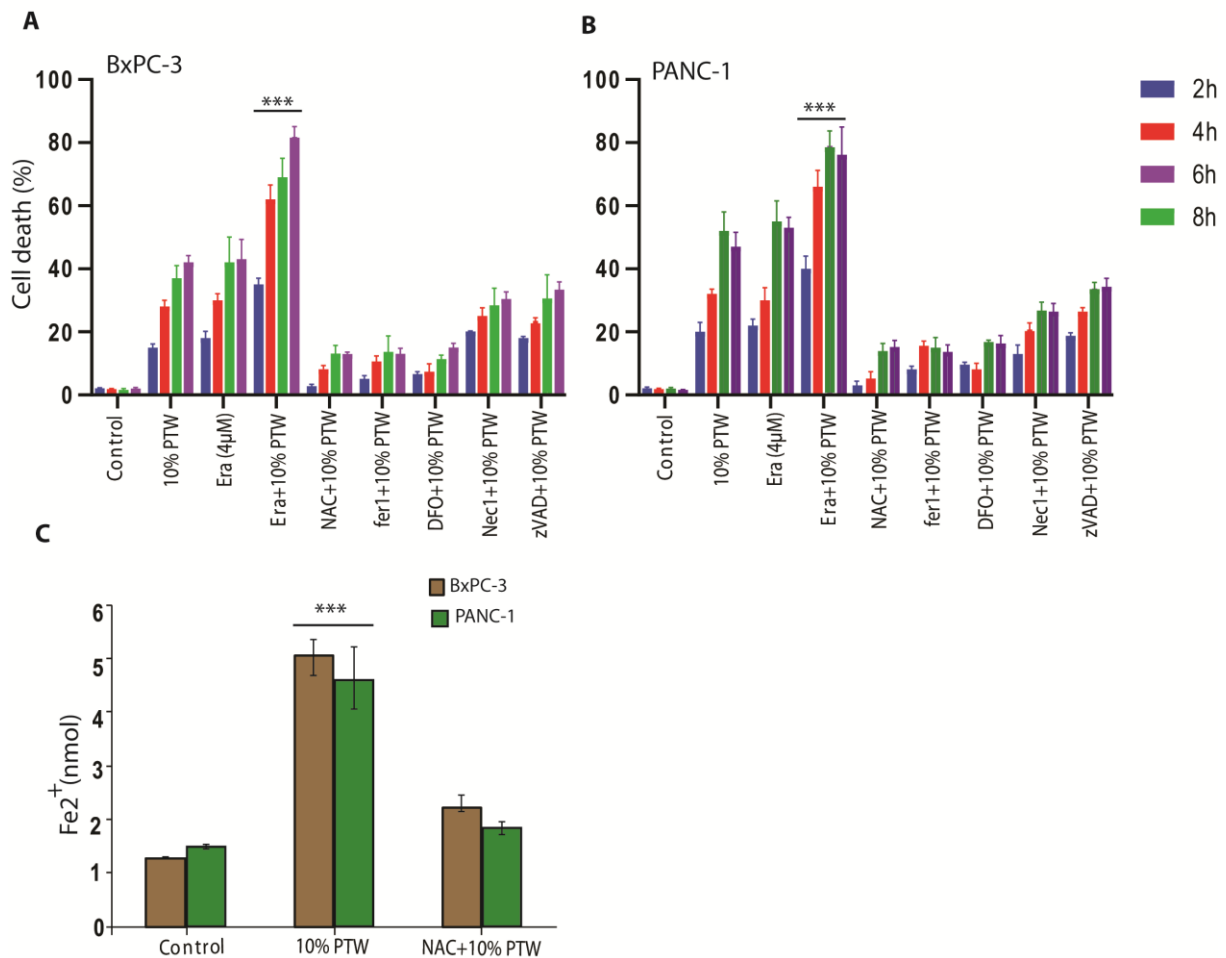


Graphical abstract

Supplementary figure and table Legend

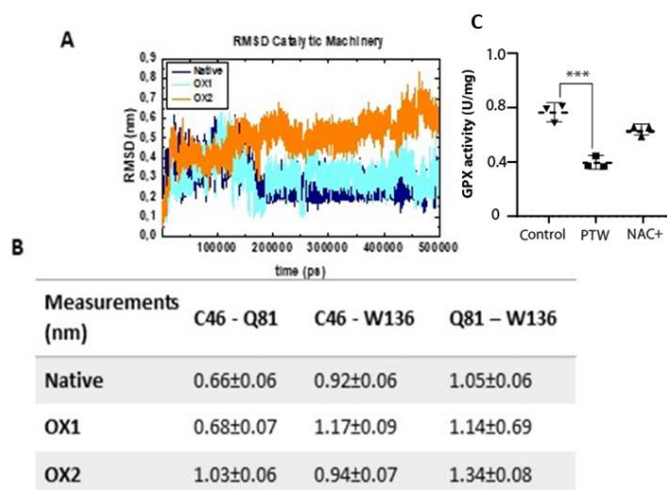


Supplementary Figure 1. Treatments were performed using a kINPen® IND plasma jet supplied with argon gas (purity 99.9%) with a flow rate of 3 LPM. The plasma is generated by high frequency sinusoidal voltage of around 2–6 kVpp to the central electrode, with a frequency between 1.0 and 1.1 MHz and a maximum power of 3.5 W. To control the temperature, the device operates as a switch off and on mode with a frequency of 2.5 kHz. The plasma is created inside the capillary and creates a plasma effluent with a length of 9–12 mm from the 1mm diameter with the gas flow towards the open side of the device. 1000 μ l of deionized water was used for the plasma treatments (10 min), with the distance of 10 mm between the nozzle of the plasma jet device and the liquid surface in 24-well plates. After exposure different PTW were applied for antitumor activity and related signaling network analysis.



Supplementary Figure 2. Effect of Plasma-treated water (PTW) on (A) BxPC-3 and (B) PANC-1 cells, bar graph representing percentage of cell death, as measured by the CellTox™ Green Cytotoxicity Assay kit, after incubation with 10% PTW, Era (4 μM), the ROS scavenging agent NAC (2 mM), the ferroptotic cell death inhibitors Fer-1 and DFO, necroptosis inhibitor Nec-1(50 μM) and caspase inhibitor zVAD (10 μM); (C) Measurement of Fe²⁺ in BxPC-3 and PANC-1 cells upon 10% PTW treatment and the ROS scavenging agent NAC treatment. The results are derived from three independent biological replicates and are shown as mean ± standard error of the mean (SEM). Statistical analysis was performed using Student's t-test with Welch's correction, *** = p < 0.001. PTW: Plasma-treated water, Era: Erastin, ROS: Reactive

oxygen species, NAC: N-Acetyl-L-cysteine, Fer-1: Ferrostatin, DFO: Deferoxamine, zVAD: benzyloxycarbonyl-Val-Ala-Asp-fluoromethyl ketone (z-VAD-FMK)



Supplementary Figure 3. (A) *RMSD* analysis of the catalytic machinery of the native, OX1 and OX2 GPX4 structures during 500 ns, (B) analysis of the alpha carbon distances between the amino acids in native as well as oxidised states and (C) GPX enzymatic activity measurement upon 10% PTW and the ROS scavenging agent NAC treatment. Statistical analysis was performed using Student's t-test with Welch's correction (b, c, d). *** = $p < 0.001$.

PTW: Plasma-treated water: Reactive oxygen species, NAC: N-Acetyl-L-cysteine